ACS OMEGA

Article

http://pubs.acs.org/journal/acsodf

Cancer Therapeutic Proficiency of Dual-Targeted Mesoporous Silica Nanocomposite Endorses Combination Drug Delivery

Chandran Murugan,[†] Srinivasan Venkatesan,[†,‡] and Soundarapandian Kannan*[,†]

[†]Division of Cancer Nanomedicine, Department of Zoology and [‡]Department of Environmental Science, Periyar University, Salem 636 011, Tamil Nadu, India

Supporting Information

ABSTRACT: The cargo-loaded mesoporous silica nanoparticles (MSNs) with convenient surface modification can facilitate the development of the innovative nanodrug system. Herein, the present investigation described the electrostatically self-assembled MSNs as a nanosized drug carrier to realize potent synergistic chemotherapy based on the specificity in targeting cytoplasm and nucleus of tumor cells. In this context, the primarily constructed MSNs were subjected with anticancer drug topotecan (TPT) into its large pores. Then, the selective TAT peptide (a nuclear localization signal peptide) was anchored onto TPT-loaded MSNs (TPT-MSN). Subsequently, the positive surface of TPT-MSN-TAT was capped with negatively charged components, poly(acrylic acid) (PAA)-cRGD peptide and citraconic anhydride (CAH)-metformin (MT), and acted as a smart gatekeeper. Comparatively, PAA-cRGD attached onto MSNs serving as the targeted molecules could upsurge by invasion into cancer cells. Interestingly, the acidic pH of the lysosomal compartment in tumor cells triggers the conjugated CAH from the polymer decorated mesoporous silica (PMS) nanocomposite and could efficiently release MT into the cytoplasm. Consequently, the remaining TPT-MSN-TAT efficiently targets the nucleus and delivers the TPT to improve synergistic chemotherapeutic effects. The precisely released drugs were individually enhanced in the *in vitro* and *in vivo* cell killing efficiencies. Thus, the study provides a potential drug delivery podium through combined drugs to realize cancer cell targeting approach.

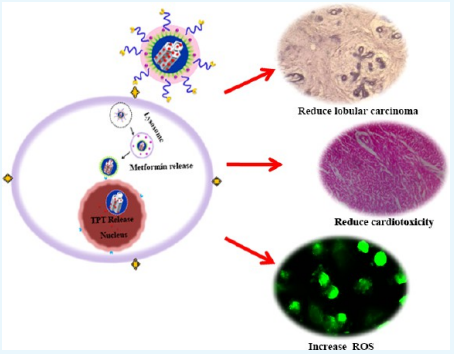

INTRODUCTION

The development of cancer therapy with the capability of selective therapeutic agent's delivery into cancer cells is one of the most attractive strategies to improve cancer treatment.[1] Of late, drug design research highly encourages the nanoparticle-dependent combination chemotherapy, and still, it is a valid option for cancer treatment. In this regard, multivalent antitumor drugs have been used together through a single nanoscopic system which may afford a significant synergistic effect against breast cancer cells with prominent cytotoxicity.[2,3] Recently, Kang et al. have developed a tumor targeting liposome assisted combination of dihydroestemisia (DHA) and doxorubicin (DOX) to overcome the drug-resistant colon cancer cells.[4] Another promising strategy developed by Zhang et al. through encapsulation of paclitaxel (PTX) and tetrandrine (TET) inside the drug carrier offers efficient multidrug-resistant cancer therapy.[5] Comparatively, most of the previously reported codelivery systems have increased the attention in discharging the combinational drugs extensively in the cytoplasm, and except in the nucleus, this kind of delivery behavior is more favorable to reducing combination effects and strong utility of those drugs.[6,7] The effective antitumor efficacy of nanomedicine at a clinically prescribed dosage is quite tedious to generate new nanoformulation for a combating drug delivery. More precisely, the delivery of drugs to the targeted regions (nucleus and cytosol) individually enhances the treatment strategy of cancer.[8] In spite of thise, many researches have given attention to the controlled release of cargos with the tunable properties of mesoporous silica nanoparticles (MSNs) as an agreeable nanosystem in the interdisciplinary research of nanomedicine. In particular, MSNs are more prevailing pharmaceutical nanoscopic drug delivery containers with respect to their large tunable porosity, extraordinary pore volume, extended surface regions, good biocompatibility, and leniency functionalized with various molecules.[9,10] Thus, they provide numerous possibilities to determine the amount of drug and site-specific release of cargo in controlled manner for the enhanced cancer therapy.[11] Most of the existing reports have focused on the dual drug loaded MSN to pursue specifically as stimuli-responsive releasing chemotherapeutic drugs at the tumor sites.[3,12] The pH sensitivity of the nanocomposite is one of the "added advantages" to release the drug into targeted sites. Moreover, the optimum pH that triggers the drugs to draw out from nanomaterials for the site-specific release of drug molecules into the tumor cells is the "guest to ghost" (cancer cells) phenomenon. The clinical success of chemotherapeutic drugs depends upon the right selection of cargo as well as their ability to release drugs into

Received: July 12, 2017
Accepted: September 19, 2017
Published: November 15, 2017

DOI: 10.1021/acsomega.7b00978
ACS Omega 2017, 2, 7959−7975

Scheme 1. Schematic route postulate the dual drug loading possibilities in PMS nanomaterials that exhibit precise drug releasing behavior in the distinct subcellular regions of cancer environment that improve cancer therapy with synergistic effects

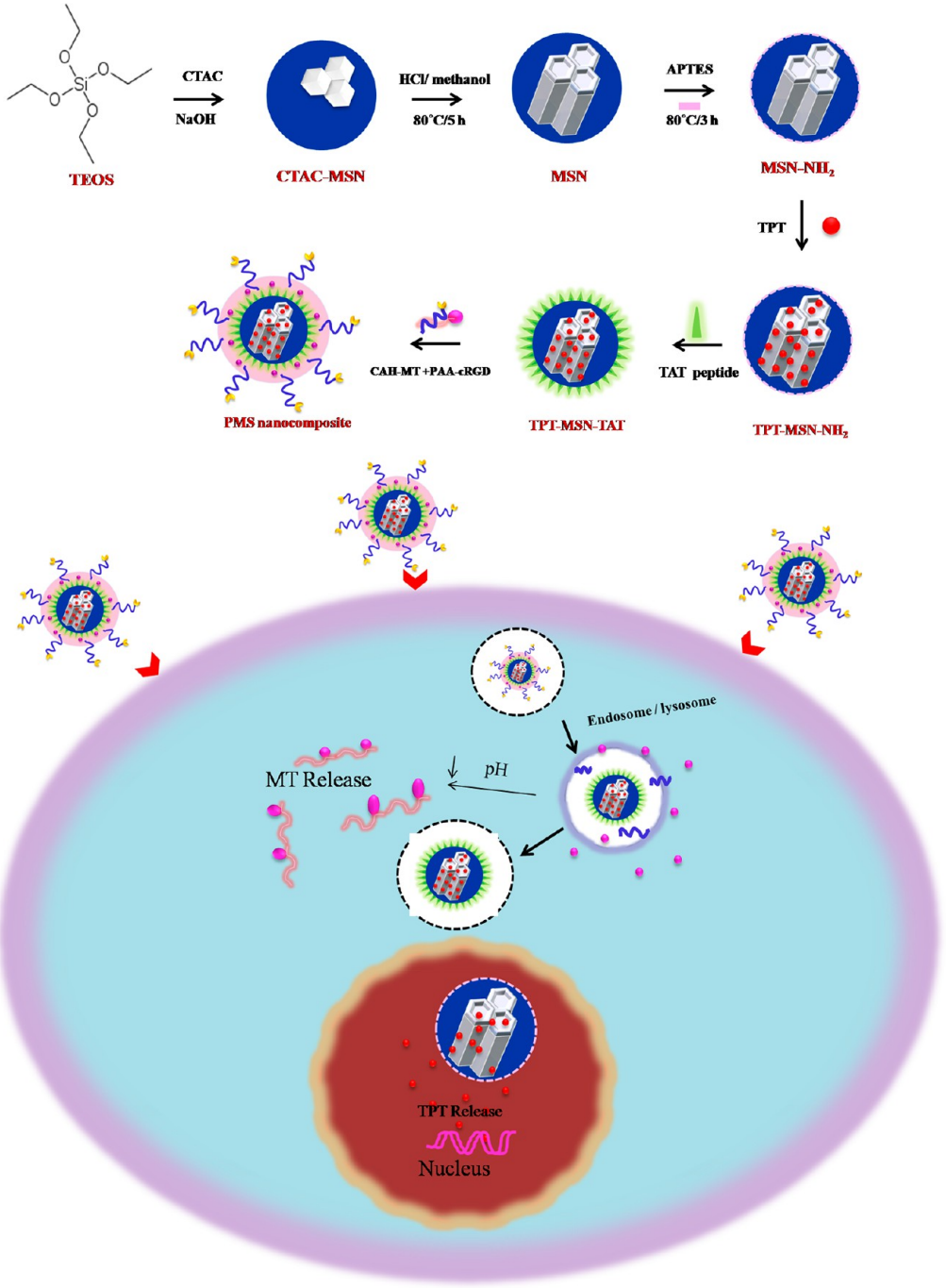

targeted tissues/cells. Moreover, a tumor vasculature homing peptide, arginine-glycine-aspartic acid (cRGD) influenced the cancer cell endocytosis and particle accumulation by recognizing its counterpart on the tumor cell membrane which is overexpressed on many cancer cell surfaces.[13]

In view of the above, the present study pertains to a new approach of self-assembly and polymer-decorated mesoporous silica (PMS) nanocomposites for the intelligent subcellular (cytosol and nucleus) delivery of model anticancer drugs. The siliceous small pores of MSN were loaded initially with topotecan (TPT), and then, the surface of the TPT-MSN was modulated by TAT (a nuclear localization signal peptide) and has the ability to transport TPT inside the subcellular nucleus via the connection with the import receptors (importin α and β (karyopherin)) on nuclear pore complexes (NPCs) with a diameter ranging from 20 to 70 nm.[14−18] In addition, PAA-cRGD and CAH-MT were subsequently capped on the surface of TPT-MSN-TAT, denoted as PMS nanocomposites. The PMS nanocomposite with cRGD peptide influences their internalization by cancer cells through interaction between the cRGD peptide and integrin receptor. Later, the CAH gets dissociated at acidic pH, which enhances the steadily release of MT, and afterward, the TAT-conjugated PMS nanocarriers act as a DNA disruptor by transport of anticancer drug (TPT) into

DOI: 10.1021/acsomega.7b00978
ACS Omega 2017, 2, 7959−7975

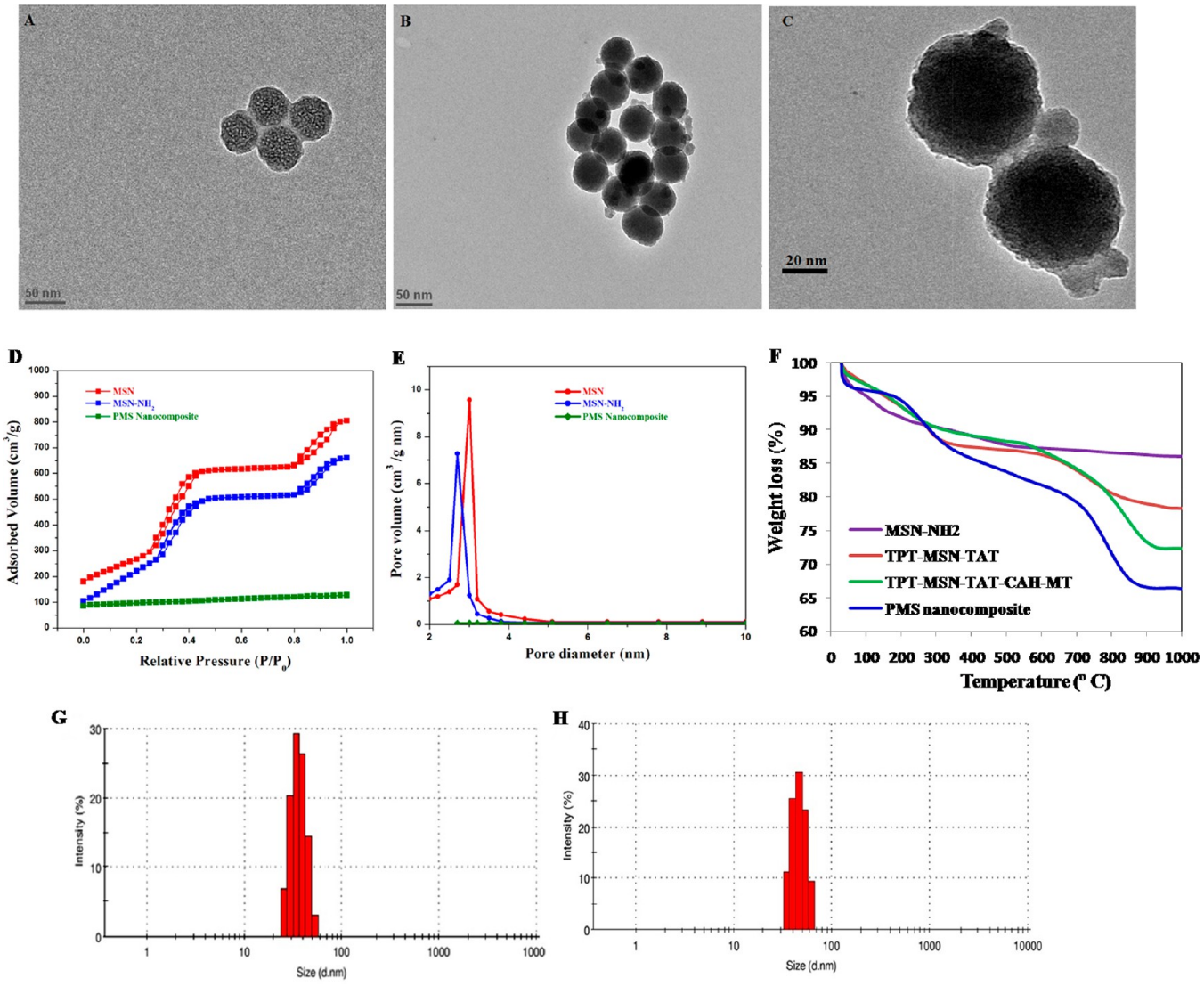

Figure 1. (A) TEM micrograph of MSN with clear microchannels. (B) and (C) TEM micrographs of PMS nanocomposite consisting of dark gray outer region exploring the polymer-coated surface-functionalized PMS and (D) N_2 adsorption/desorption isotherms and (E) the porosity characters of synthesized MSNs, MSN-NH_2, and PMS nanocomposites evaluated by BJH and BET analysis. (F) TG analysis of MSNs, MSNs-NH_2, TPT-MSN-TAT-CAH-MT, and PMS nanocomposites. (G) The mean hydrodynamic diameter of MSN and (H) size measurement of PMS nanocomposite by dynamic light scattering (DLS).

the nucleus. Moreover, the *in vitro* synergistic effects and intracellular drug release, targeted ability, subcellular distribution, and *in vivo* therapeutic efficiency were performed to investigate the effects of the PMS nanocomposite.

RESULTS AND DISCUSSION

To construct versatile nanosized mesoporous silica nanocomposites, the MSN-NH_2 was foremost prepared by the base-catalyzed sol−gel process. The synthesis procedure is outlined in Scheme 1. The MSN-NH_2 has plenty of pores used to accommodate the enormous amount of topotecan (TPT) by a simple diffusion process. Subsequently, the amino-functionalized MSN surface was modified by FITC-labeled TAT peptide to obtain TPT-MSN-TAT. Then, PAA-cRGD and CAH-MT were added (1:3 ratio) and adsorbed onto the outer surface of TPT-MSN-TAT through electrostatic forces. The cRGD offers a tumor targeting agent that obviously thwarts cancer cells through cRGD−$\alpha v\beta 3$ interaction. At this crisis, acidic pH (4.8−5.5) encourages the release of a second drug MT from CAH through electrostatic repulsion. Consequently, TPT-MSN-TAT influenced nuclear internalization, and the driving force pushed the cationic TPT away from the MSNs within the nucleoplasm. The result evidenced that the PMS nanocomposite could emerge as an agreeable nanodrug system to induce synergistic chemotherapy via expected delivery of cargo directly in cytosol and nucleus compartments as reported.[8] In TEM analysis, Figure 1A shows a discrete, spherical morphology of MSNs with a diameter ranging from 43 to 50 nm, and also the large deep-rooted pore structures evenly distributed in the core of MSNs were observed. The TEM micrographs in Figure 1B and 1C show the thickness as well as a thin gray outer layer around the MSN, which entails the presence of organic moieties that covered the MSN core−shell and PMS nanocomposites, thereby producing a range between 45 and 54 nm in diameter. In addition, almost all the pores on the MSNs were filled with drug moieties which were confirmed through TEM analysis. The previous report suggested that the diameter of MSN-TAT was around 50 nm

DOI: 10.1021/acsomega.7b00978
ACS Omega 2017, 2, 7959−7975

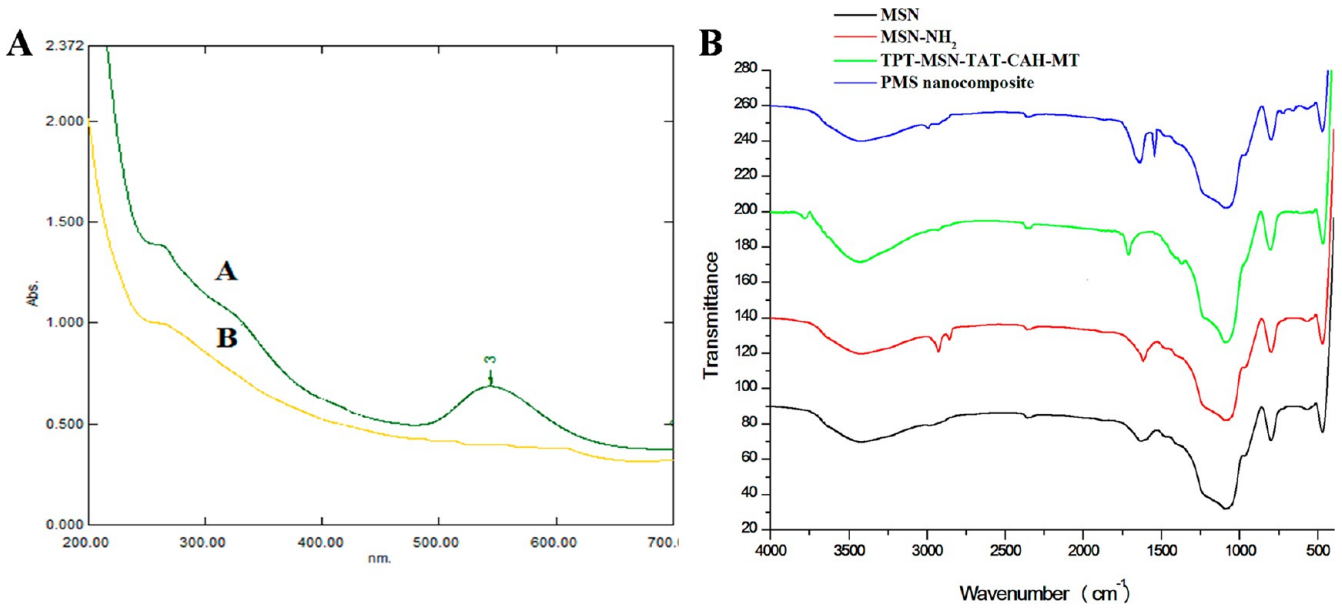

Figure 2. (A) UV−vis spectra of TAT-conjugated MSNs earlier than and later than centrifugation. (B) FT-IR of MSNs after the removal of surfactant CTAC (black), MSN-NH_2 (red), TPT-MSN-TAT-CAH-MT (green), and PMS nanocomposite (blue).

or smaller, which could enhance selective nuclear uptake and subsequently deliver the active anticancer drug that leads to cancer cell lethality.[19] Further, the nitrogen adsorption and desorption measurements (Figure 1D and 1E) were recorded with their respective surface area, pore volume, and pore diameter. These parameters get decreased progressively after every amendment during synthesis of PMN nanocomposites. The bare MSN exhibited their surface area (805 $m^2\ g^{-1}$), pore volume (1.44 $cm^3\ g^{-1}$), and narrow BJH pore size distribution (average pore diameter 3.0 nm), whereas MSN-NH_2 resulted in 660 $m^2\ g^{-1}$, 0.88 $cm^3\ g^{-1}$, and 2.7 nm, respectively. The gradual decrease in the pore volume and pore size indicates the modification of MSN surface by the amine groups. Simultaneously, the surface area and pore volume of PMS nanocomposites had been reduced to 92 $m^2\ g^{-1}$ and 0.31 $cm^3\ g^{-1}$, respectively, which further revealed the dominance of organic moieties mostly in the surface of the particles. The percentage of nanoformulations was determined by thermogravimetric analysis (TGA). As depicted in Figure 1F, following heating to 1000 °C, the percentage of weight loss of MSN-NH_2 was displayed as 14.9%, which was increased to 21.7% after the TAT modification. The weight loss of TPT-MSN-TAT-CAH-MT and PMS nanocomposite obviously showed a considerable weight loss of 27.6% and 33.6%, respectively. The TGA effect of PMS nanocomposite had 5.9% greater weight loss than that of TPT-MSN-TAT-CAH-MT, which could ensure the decomposition of functionalized components (PAA-cRGD). The data depicted in Figure 1G displayed that the average hydrodynamic diameter of MSNs at pH 7.4 was 46 nm with a value of 0.1 polydispersity index (PDI). Additionally, Figure 1H confirms that the average particle size of PMS nanocomposites was 47.7 nm, with a minimal PDI of 0.03 and the greatest monodispersity condition. It is noted that the size is slightly larger than MSN. It proves to be a successful packing and conjugation of drug molecules and polymers in pores and the surface of functionalized MSNs. As mentioned earlier, a tiny nanosized particle is a substantial drug that can enter across nuclear pore complexes (NPCs); thus, the tiny sized PMS nanocomposite provides an excellent drug delivery.[18,20]

As in Table S1, the ξ potential of the silanol functional group of MSN was negatively charged (−26.7 mV) at pH 7.4, and the MSN-NH_2 was a positively charged surface (+20.4 mV) since the external silanol group was instituted to ingest the surface charge of the particles which was shifted from −26.7 mV to +20.4 mV. Following grafting with TPT onto TPT-MSN-TAT leads to the dramatic increase in surface charge (+28.1 mV). Following, the TPT-MSN-TAT are modified with negatively charged PAA+cRGD with CAH+MT layers, and the potential changes from +28.1 mV to +18.4 mV. As depicted in Figure S1, the stability of the PMS nanocomposite in 10% mouse serum (mSerum) suspended in DMEM or 0.01 M of PBS (pH 7.4) exhibits a small size change after 48 h. Interestingly, the obtained result reveals that the prepared PMS nanocomposite was found to maintain its integrity and stability under the physiological pH for 48 h (2 days). Generally, MSNs with positive charge seem to be endocytosed more rapidly since this might be expected to bind negatively to the charged cell surface.[21] Moreover, the previous literature indicates the positively charged nanoparticles exhibit prolonged circulation with improved retention time. Further, Wim et al. and Andre et al. are in agreement with our hypothesis that the positive charge of the nanoproduct could play an outstanding role in delivery of drugs and other ligand molecules.[22,23]

As shown in Figure 2A, the UV−vis absorbance was conducted for the preliminary conformation of TAT modification on MSN-NH_2. Further, this was clearly depicted by the appearance and disappearance of the characteristic peak of fluorescene isothiocyanate (FITC) conjugated at the N-termini of the TAT onto MSN. Presently recorded results are in support with the previous report on successful modification of the MSN surface with FITC-labeled TAT.[19] From Fourier transform infrared (FTIR) spectroscopic analysis (Figure 2B), the complete removal of surfactant CTAC from MSN was clearly confirmed by the disappearance of the C−H peak in the spectrum wavelength range (3000−2800 cm^{-1}) for the CTAC-extracted MSNs. Subsequently, characteristic peaks observed in the spectrum of MSN-NH_2, the peak at 1583 cm^{-1} expectedly to the stretching vibration of $-NH_2$ bending, and the

DOI: 10.1021/acsomega.7b00978
ACS Omega 2017, 2, 7959−7975

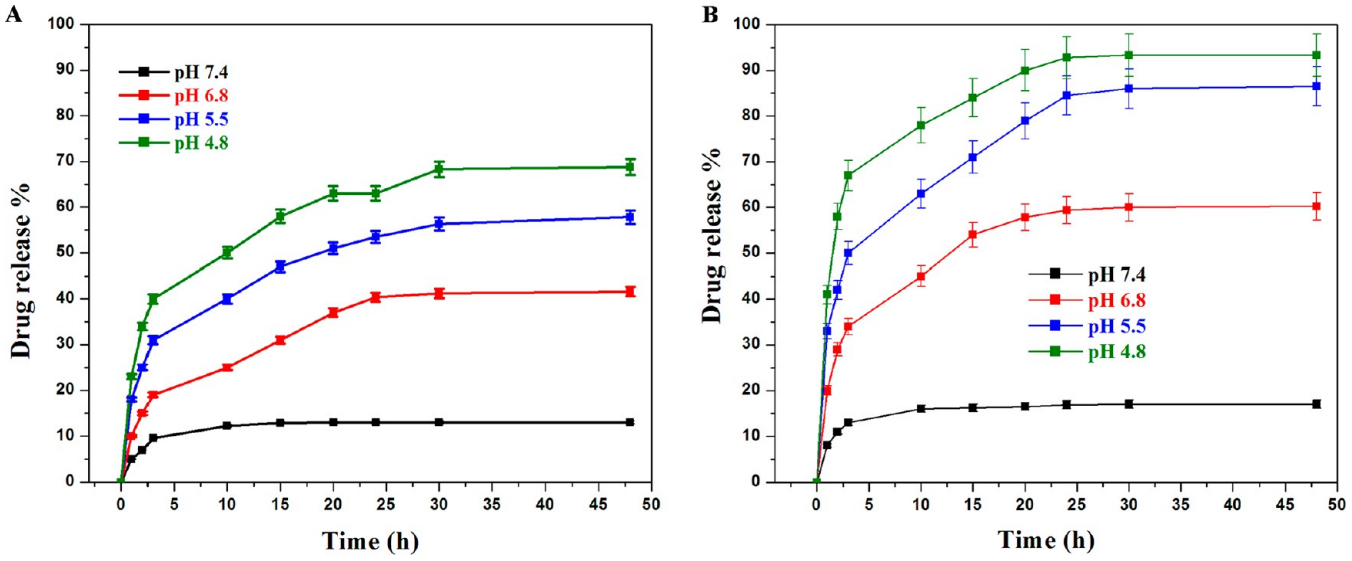

Figure 3. pH-dependent *in vitro* drug discharge behaviors of dual drug encapsulated PMS nanocomposites at various pH values (7.4, 6.8, 5.5, and 4.8). (A) Drug release profile of TPT and (B) MT release profile from PMS nanomaterials at different pH value for 48 h. Error bars represent the standard error (SE) of the mean from triplicate experiments.

appearance of C−H stretching vibrations at 2930 cm^{-1} were confirmed by the presence of amine groups on the surface MSNs. As-prepared TPT-MSN-TAT-CAH-MT displayed the new peaks at 1553 and 1718 cm^{-1}, which could belong to the N−H bending vibration of CAH-MT. Final modification with PAA-cRGD on the surface of TPT-MSN-TAT-CAH-MT provides the C═O stretching vibration in the amide group and the C═O stretching vibration in the carboxyl group, respectively, which indicates the successful grafting of PAA-cRGD on the surface of TPT-MSN-TAT-CAH-MT, denoted as the PMS nanocomposite.

DRUG LOADING

The present result disclosed that the obtained MSNs have high intrinsic pore volume that could be used to encapsulate the anticancer drugs with high loading efficiency. The loadings of TPT and MT on MSNs were achieved based on the principle of adsorption and hydrophobic interaction, and this result was in agreement with the earlier report.[24−26] Despite this, the TPT (positively charged) maintains electrostatic interaction with SiO^- (negatively charged) groups in MSN pores at physiological pH. The second drug MT was trapped into the CAH. The positively charged surface of TPT-MSN-TAT was functionalized with negatively charged CAH with MT by the electrostatic interaction. The drug uptake property and encapsulation efficiency of PMS nanocomposites were found to be 15.5 and 87.5% for TPT and 20.1 and 77.7% for MT, respectively. Thus, the PMS nanocomposite possesses both high drug loading capacity and releasing efficiency and could induce high rate of cytotoxic effects on cancer cells.[27,28]

DRUG RELEASE

To evaluate the potential releasing property of TPT and MT from PMS nanocomposites, the PMS nanocomposites were dissolved in PBS buffer solution at different pH (7.4, 7.3, 6.8, 5.5, and 4.8) for up to 48 h at 37 °C. Figure 3A shows the drug release rate of TPT, and Figure 3B explains MT release behavior from the PMS nanocomposite. Further inspection manifested that approximately 13.1% of TPT was released at the pH of 7.4 within 48 h, whereas the MT release profile was recorded as 17.3% in 24 h. At pH 7.4, the discharge behaviors of drugs was lowered from PMS nanocomposites, which indicates that the surface and the openings of mesopores of MSNs were tightly capped by PAA and CAH-MT. Remarkably, at 48 h, the TPT and MT release was recorded as 41.6% and 60.2% at pH 6.8, respectively. Interestingly, at pH 5.5 and 4.8, the release rates of TPT (57.61% and 88.8%) and MT (68.8% and 93.3%) were calculated, respectively. Nevertheless, the present findings clearly demonstrated that both drugs are released at a higher rate at pH 5.5 and pH 4.8, due to the rapid dissociation of the CAH and PAA from TPT-MSN-TAT to accelerate the drug release. To gain insights into the process of dissociation and acceleration, the underlying pH-dependent drug release might occur by an altered interactive force between drug molecules and PMS nanocomposites. Surprisingly, at pH 5.5 and 4.8 (endosomal and lysosomal pH), the negatively charged CAH is protonation; it could trigger the reversal conversion of the negatively charged CAH into positively charged citraconic acid; and it causes the electrostatic interaction between CAH-MT to stimulate the release of MT at the cytoplasm from PMS nanocomposites. Then, detachment of CAH-MT and PAA layers influences the exposure of amine-functionalized TPT-MSN-TAT (small size <50), and the conjugated TAT peptide facilitates the intranuclear distribution through the nuclear pore complexes. As depicted in Figure S2, normally the cell nucleus had a pH of ≈7.3,[29] and at this condition, the carboxylic group in TPT (pK_a = 11.7) causes electrostatic repulsion with negatively charged mesoporous structure (SiO−) and could trigger the TPT remaining in the MSNs-TAT to be discharged within the nuclei. The antineoplastic activity was enhanced along with the increase in the intranuclear TPT concentration.[26] The discharged amount of TPT from TPT-MSN-TAT was calculated as 52.5% for 48 h at 37 °C. Thus, the present findings are in agreement with the earlier reports that strongly emphasize the notion that the drug loading and release are pH-dependent processes.[30−32] The premature discharge behaviors of TPT and MT from the PMS nanocomposite at pH 7.4 were found to be limited. This might

DOI: 10.1021/acsomega.7b00978
ACS Omega 2017, 2, 7959−7975

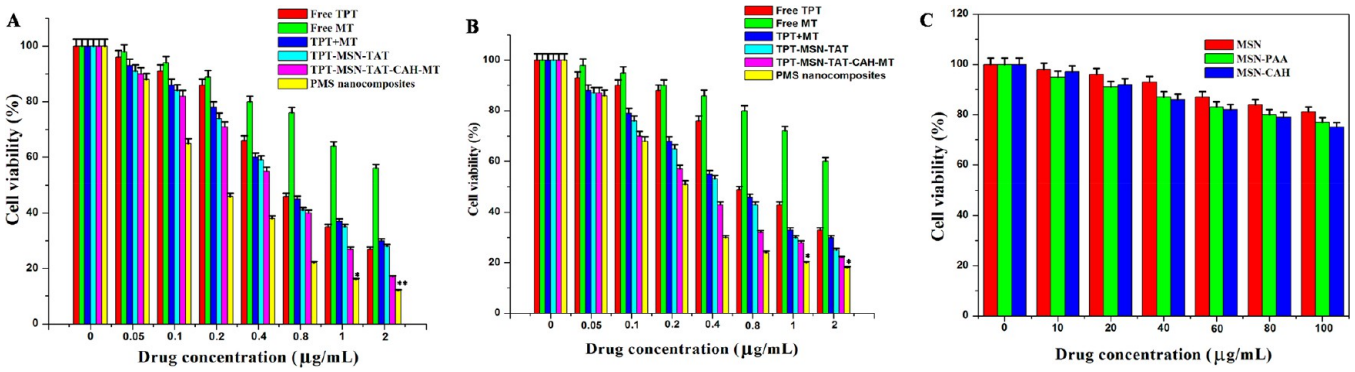

Figure 4. *In vitro* cytotoxic effects of nanodrug formulated on (A) MDA-MB-231 and (B) MCF-7 breast cancer cells incubated with different concentrations. (C) Cytotoxic effects of HBL-100 normal breast cells at various concentrations of MSN and MSN-PAA and MSN-CAH. The data showed a mean ± standard error (SE) of the mean (n = 3), and *$p \leq 0.05$ value assumes statistically significant.

effectively decrease the undesired side effects in normal tissues, while these nanocomposites are in circulation. The pH-sensitive drug discharge capabilities are perfectly sponsored by an endocytosis process. Moreover, there is increasing evidence to support the hypothesis of the present study that the discharge of drug in an acidic environment (pH 4.8−5.5) might enhance the therapeutic benefits of the PMS nanocomposite in cancer treatment.[33,34] Together with the slow and steady discharge profile of TPT at the nuclear pH from PMS nanocomposites by active nuclear transport via TAT targeting, this induces sustained discharge of TPT thereafter.

***In Vitro* Cytotoxicity.** The cytotoxicity of TPT, MT, TPT +MT, TPT-MSN-TAT, TPT-MSN-TAT-CAH-MT, and PMS nanocomposites was quantitatively evaluated by MTT assay. The various concentrations (0.05−2 μg/mL) of drug and nanoformulations were incubated with MDA-MB-231 and MCF-7 breast cancer cells for 48 h to evaluate the cytotoxic effects. As shown in Figure 4A and 4B, the cytotoxicity of various nanoformulations was also investigated. The cell cytotoxicity of TPT+MT on both cancer cells was observed and showed a significant increase as compared to free drugs (TPT and MT). The IC_{50} values of TPT+MT were found to be 0.623 μg/mL and 0.54 μg/mL, whereas the TPT accounts for 0.71 μg/mL and 0.65 μg/mL, for cancer cells (MDA-MB-231 and MCF-7 cells), respectively. This cytotoxic effect could be attributed to the synergistic effects of combination drugs on the cell viability at different incubation periods. The IC_{50} value of TPT-MSN-TAT-CAH-MT was found to be 0.45 μg/mL and 0.37 μg/mL, for MDA-MB-231 and MCF-7 cells, respectively, which was much lower than that of TPT+MT, which could be attributed to the delayed discharge of drugs. The IC_{50} values of PMS nanocomposites (0.18 μg/mL and 0.28 μg/mL) had a lower IC_{50} value than that of TPT-MSN-TAT-CAH-MT. The IC_{50} values of the nanoformulations were listed in Table S2. The results also showed that free drug (TPT and MT) and combination drug (TPT+MT) showed better cytotoxic effects in the MCF-7 cell than MDA-MB-231 cells. On the other hand, the PMS nanocomposite shows the higher inhibitory effects on the growth of MDA-MB-231 cells than in MCF-7 cells, indicating the overexpression of integrin receptor on the surface of these cancer cells.[3] The cRGD peptide of PMS nanocomposites binds to the overexpressed $\alpha v\beta 3$ integrins on MDA-MB-231 cancer cells, leading to the uptake of nanocomposites by receptor-mediated endocytosis. Upon internalization, the PMS nanocomposite subsequently releases TPT and MT in the cytosol, and the nucleus showed increased combination effects and antiproliferative activities against cancer cells (MCF-7 and MDA-MB-231). Thus, the nuclear and cytoplasm-targeted drug delivery by the PMS nanocomposites accomplishes the synergistic anticancer activity. Then, the cells were incubated with MSN-PAA and MSN-CAH which exhibited lower toxic effect than free drugs, revealing the biocompatible nature of PMS nanocomposites (Figure 4C), that could effectively deliver dual drugs into the cells and showed improved therapeutic activity.[3]

Confocal Laser Scanning Microscopy (CLSM) Analysis. The uptake of PMS nanocomposite by MDA-MB-231 cells was systematically studied using CLSM. There are several reports stated on integrin receptors which are found to express in tumor cells as well as breast cancer cells that specifically recognize RGD peptides.[35,36] The cRGD peptide-grafted PMS nanocomposites stimulated the selective uptake by cancer cells, and it was expected that they could more easily transport into the cancer cell membrane.[37] As in Figure 5, the specific cellular uptake was studied at different time intervals (6, 12, 18, and 24 h). In Figure 5A and 5B, after incubation with the PMS nanocomposite (IC_{50} concentration) for 6 and 12 h, respectively, there was a significant increase of fluorescent intensity in cytoplasm as compared to the nucleus. Besides, it could be observed in Figure 5C that the PMS nanocomposite significantly possesses higher percentage of cellular uptake in nucleus than in the cytoplasm, indicating FITC-labeled TAT-grafted TPT-MSN with <50 nm size enhanced nuclear internalization after 18 h. Additionally, the fluorescence image (Figure 5D) revealed that the increased amount of green fluorescence emerged in the nucleus after 24 h, which demonstrated that the TAT-grafted TPT-MSN might be completely transported inside the nucleus. As depicted in Figure 5E, FITC intensity was analyzed by a fluorescence plate reader, after PMS nanocomposite treatment in MDA-MB-231 cells. Therefore, it is assumed that the incorporation of cRGD peptide and TAT peptide on the PMS nanocomposite surface could improve the receptor-mediated endocytosis and subsequently discharged MT at the cytoplasm. Thereafter, the TAT-mediated nuclear internalization would assist the TPT to release into the nucleus.

Furthermore, the cell uptake efficacy of with or without cRGD-grafted PMS nanocomposites on MDA-MB-231 cells was examined. As shown in Figure 6A, after incubation with PMS nanocomposite in the absence of cRGD, peptide conjugation exhibits lower cellular uptake in MDA-MB-231 breast cancer cells than that of the cRGD-grafted PMS

DOI: 10.1021/acsomega.7b00978
ACS Omega 2017, 2, 7959−7975

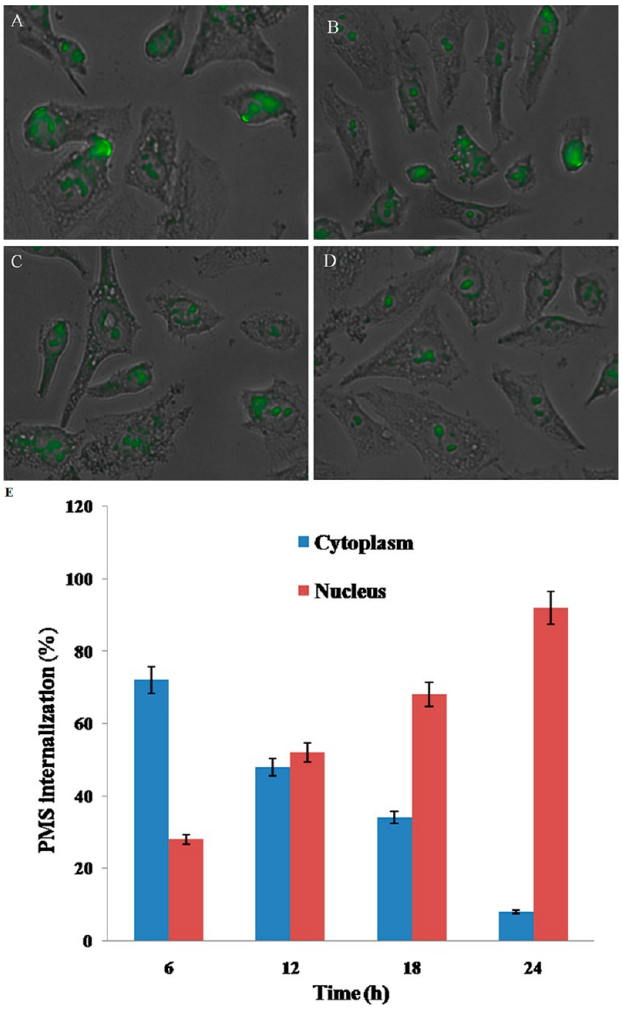

Figure 5. CLSM images of MDA-MB-231 breast cancer cells after treatment with PMS nanocomposites (IC_{50} concentration) at the different time intervals (A) 6 h, (B) 12 h, (C) 18 h, and (D) 24 h, verifying the intracellular location of FITC-labeled PMS nanocomposites. (E) Graph showing the quantitative analysis of intracellular location of the PMS nanocomposites at different time intervals.

nanocomposites, after 24 h. As depicted in Figure 6B and 6C, a significant increase of fluorescent intensity was observed in peptide-conjugated PMS nanocomposites, and the uptake of MDA-MB-231 cancer cells is twice as high as that of the PMS nanocomposite without peptide conjugation. Hence, it is expected that PMS nanocomposite with grafted cRGD improves uptake by tumor cells and enhances anticancer efficacy.[3,36]

PMS Nanocomposite Internalization by Bio-TEM Images. The PMS nanocomposite internalization into MDA-MB-231 cells was confirmed by Bio-TEM images in Figure 7. After 24 h incubation, PMS nanocomposite tethered cRGD peptide treatment could enhance the targeting of MDA-MB-231 cells. This strategy unambiguously shows the advantage of delivering the drugs into the cytoplasm and nucleus, respectively.

The bio-TEM analysis witnessed the encapsulated PMS nanocomposite and perfect delivery of drugs into the organelle level. Figure 7A and 7B clearly demonstrates that the receptor-mediated endocytosis facilitated the internalization and accumulation of spherical-shaped PMS nanocomposites.[38] The yellow arrows indicate particle internalization, whereas the pink color arrow points out the entry of the PMS nanocomposite via receptor-mediated endocytosis and accumulation as well as distribution in the cytoplasm. Meanwhile no nanocomposite was noticed in the nucleus. Typically, the PMS nanocomposite with cell-targeting ligand was internalized via receptor-mediated endocytosis, which certainly transports into lysosomes.[39] These acid vesicles are pivotal organelles to begin the pH-responsive dismantling of the PMS nanocomposite and thus switch on the intracellular functions. In Figure 7C and 7D, the red arrow illustrates numerous spherical shaped particles that could be reported in the intracellular region of the tumor cell, which demonstrated that a greater amount of PMS nanocomposites were uptaken by the MDA-MB-231 breast cancer cells. As a subsequent event of endocytosis, the PMS nanocomposite was processed in lysosomes and then eventually released the MT into the cytoplasm; afterward the polymer was disassembled, and as a result, TPT-MSN-TAT remained in cytosol. In addition, the red arrows show (Figure 7E and 7F) the accumulation of TPT-MSN-TAT that was sporadically located within the nucleus. Instead, a number of black color spherical particles were identified as nanoparticles agreeing to their shape and size, and further PMS nanocomposites exhibited effective internalization and distributions in the nucleus and released the drugs at a controlled manner.[40,41] The previous reports of Lu et al. have studied that the uptake of MSNs into HeLa cells with varied sizes from 30 to 280 nm in which they found that 50 nm sized MSNs could enter into the cancer cells, efficiently.[42] It is noteworthy that the presently obtained result suggests the functional relevance of PMS materials as a carrier for cargos such as TPT and MT release at the subcellular level.

Analysis of Nuclear Morphology by Fluorescence Microscopy. As seen from Figure 8, the effects of TPT, MT, TPT+ MT, TPT-MSN-TAT-CAH-MT, and PMS nanocomposites (2 μg/mL) on the formation of apoptotic bodies in treated MDA-MB-231 cells were investigated by fluorescence microscopy. Therefore, the cell nucleus was stained with blue luminescence fluorescent dye DAPI (left), and we determined the nuclear condensation in cell death (apoptosis). Thus, PMS nanocomposite-treated cells have condensed nucleus, nuclei chromatins, gathering, and completely fragmented nuclear bodies, indicating the apoptosis. The PMS nanocomposite induces a higher rate of antiproliferative efficacy against MDA-MB-231 cells than free drugs (TPT and MT). Furthermore, a large amount of green fluorescent emerged and randomly due to the Rh-123 (middle) distributed in the cell cytoplasm, which determines the loss of membrane potential ($\Delta\psi$m) of active mitochondria in MDA-MB-231 cancer cells. The cytotoxic effects of free drugs in the PMS nanocomposite induce instability of the mitochondrial integrity and activation of caspases, leading to cell death (apoptosis). The above results revealed that the cRGD peptide on PMS nanocomposites released MT in the cytoplasm and TPT in nucleus, subsequently providing higher apoptotis in MDA-MB-231 cells effected by induced mitochondrial dysfunction and DNA disruption.[43]

ROS Generation in PMS Nanocomposite-Treated Cells. As depicted in Figure 9A, the measurement of ROS formation in breast cancer cells during treatment with TPT, MT, TPT+MT, TPT-MSN-TAT-CAH-MT, and PMS nanocomposites was examined. The fluorescence strength of DCFH-DA stain was detected in treated MDA-MB-231 cells.

DOI: 10.1021/acsomega.7b00978
ACS Omega 2017, 2, 7959−7975

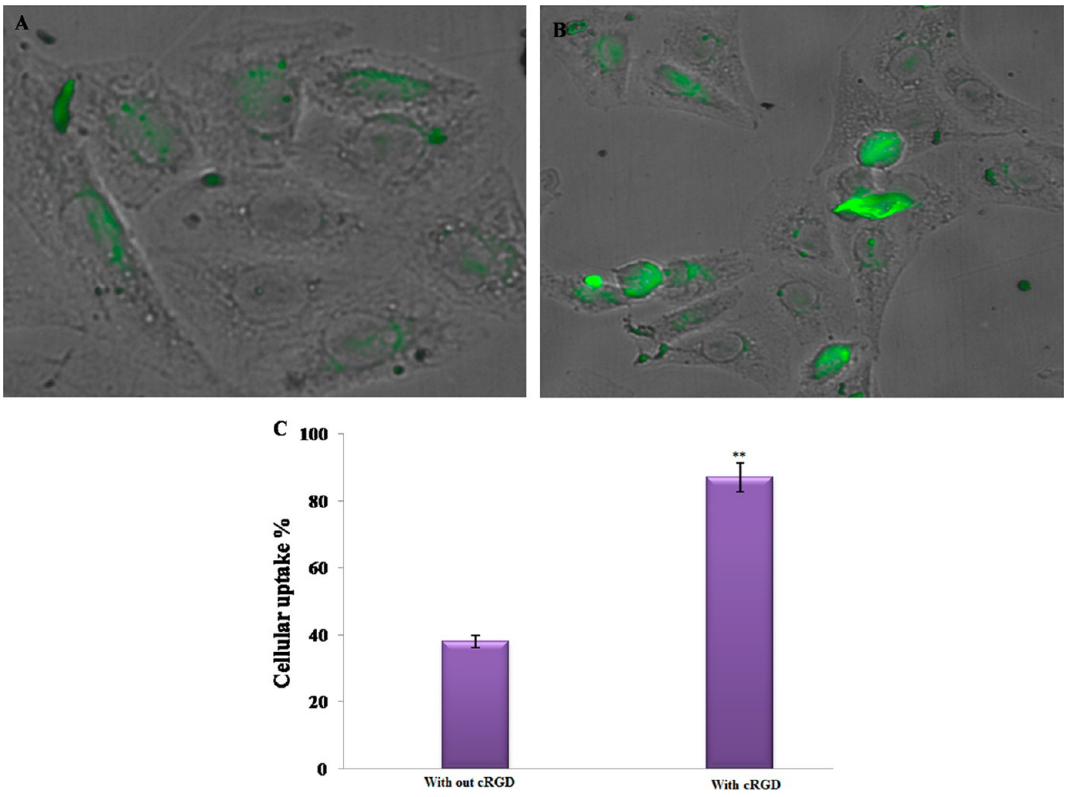

Figure 6. CLSM images of the cellular uptake efficacy (A) without cRGD-grafted PMS nanocomposites and (B) with cRGD-grafted PMS nanocomposites at the IC_{50} concentration in MDA-MB-231 cells after 24 h incubation. (C) The graph shows the cellular uptake efficacy of different nanoformulations.

Of note, 2.0 μg/mL of TPT induced formation of ROS during 24 h of treatment. Co-treatment with TPT+MT induced accumulation of ROS at a large level in cancer cells. The TPT-MSN-TAT-CAH-MT increased ROS levels, while compared with free drugs, and in spite of using targeting agents together, the content of ROS is altered significantly. In contrast, the ROS level was increased within 24 h in the cancer cell. These results indicate that the dual-targeted PMS nanocomposites with targeted agent (cRGD) elevate ROS generation synergistically. These results suggest the PMS nanocomposite-mediated drugs distributed into tumor cells generate ROS as well as DNA damage leading to apoptosis. Hence, the PMS nanocomposites were considered as the most worthy materials to proficiently induce the ROS production to activate intrinsic apoptotic proteins in cancer cells. Then, ROS intensity was evaluated by a fluorescence plate reader (Figure 9B) in PMS nanocomposite-treated MDA-MB-231 cells. Hence, the productions of increased levels of ROS play a crucial function in the regulation of cell apoptosis.[44]

Flow Cytometry Analysis for Apoptosis. The MDA-MB-231 cells were treated with free TPT (46.72%), TPT+MT (52.15%), TPT-MSN-TAT-CAH-MT (73.62%), and PMS nanocomposites (86.2%), and the IC_{50} values after 48 h were subjected to staining with Annexin-V-FITC/PI dual fluorescence staining, which discriminated the apoptotic cells from live cells (Figure 10A–E). Annexin V-FITC, a specific apoptotic marker that could be bound to cells in early apoptosis and propidium iodide (PI), binds to late apoptotic cells, even when the cells are dead.[45,46] The control cells showed slightly apoptotic activities (<5%), when compared to the free drug, and after treating with the combined drugs (TPT+MT) could induce more apoptotic cells in the case of cancer cells. Figure 10F shows the treatment effects of nanodrugs on MDA-MB-231 cells. Additionally, the PMS nanocomposites exhibit more specifically tumor-targeted ability and effective delivery of combined drugs at distinct tumor subcellular regions that could enhance synergistic antitumor activity, resulting from higher induction of apoptosis.[47,48]

***In Vivo* Cancer Treatment.** The *in vivo* antitumor effects of the normal saline, TPT, MT, TPT+MT, TPT-MSN-TAT, TPT-MSN-TAT-CAH-MT, and PMS nanocomposites, were evaluated at a dose of 5 mg/kg body weight during the intravenous injection of the breast tumor bearing mice. As depicted in Figure 11A, the tumor volume was recorded as 1113.00 $\pm$ 0.11 mm^3 in saline-treated mice at the end of the 24th day. Mice treated with TPT (750.05 mm^3), MT (890 mm^3), and TPT+MT (555 mm^3), respectively, showed modest tumor growth suppression compared to the saline-treated group. Interestingly, the tumor growth was noticed as 430 mm^3 in TPT-MSN-TAT-CAH-MT treated mice. However, the enhanced tumor inhibition occurred in the mice groups treated with PMS nanocomposites (163 mm^3), due to the improved cellular targeted efficiency of the PMS nanocomposite. As in Figure 11B, the body weight of mice was calculated after each treatment. Mice administrated with saline, TPT-MSN-TAT-CAH-MT, and PMS nanocomposites exhibited a gradually increasing body weight, demonstrating the harmless nature of those materials. In contrast, the mice treated with TPT had decreased body weight compared to the control group. No adverse effect was noticed in the selected vital organs of the animals treated with PMS nanocomposites as similar to control. Besides, the organ damage and tissue disintegration were

DOI: 10.1021/acsomega.7b00978
ACS Omega 2017, 2, 7959–7975

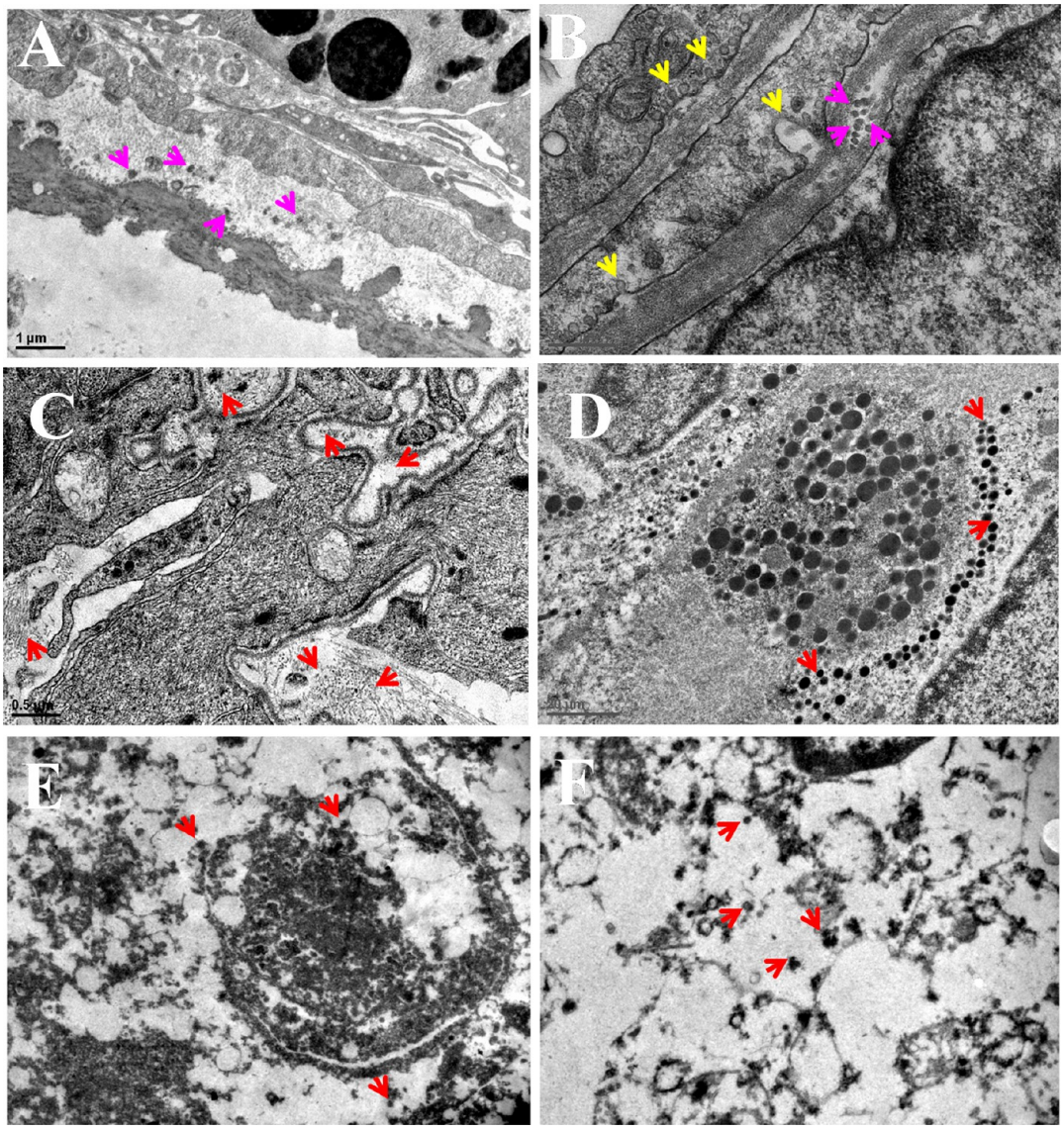

Figure 7. *In vitro* cellular uptake of PMS nanocomposites by MDA-MB-231 cells witnessed the accumulation of nanocomposites in the cytoplasm and nucleus. (A) and (B) TEM image reveals PMS nanocomposites get internalized into the cell membrane through receptor-mediated endocytosis. (C) and (D) TEM images of PMS nanocomposites distributed within the cancer cells. (E) and (F) The PMS nanocomposites distributed throughout the nucleus. Red arrows point out the distribution of spherical shaped PMS nanomaterials. Scale bar = 1 μm.

observed in free drug (TPT) treated animals with the recommended doses (Figure 11C). Together, considering the data presented in histopathology studies are in perfect agreement with the previous literature underlines that the TPT-treated mice group showed obvious organ damage of necrosis in kidney and heart tissues compared to the saline and PMS nanocomposite treated mice group.[49−51] Though several surface modifications have been employed in the preparation of MSN to provide the desired properties, viz., toxicity, biodegradability, biocompatibility, and targeted drug delivery, the half-life of the materials in circulation, excretion, and degradation are the concerns to determine the safety of materials.[52,53] As depicted in Figure 11D, the ratio of tumor concentration and liver concentration was 5.9. In the case of PMS nanocomposites, the concentration of TPT in tumor tissue was 2.96 times higher as compared to TPT. The enhanced circulation time, as well as specific uptake of PMS nanocomposites to $\alpha v\beta 3$ receptors, could actively reduce the tumor growth. The TPT concentration in the heart, lungs, and kidney for the two formulations was not significant. This sequential investigation highlights the need for novel silica-based nanocomposites to carry dual drugs with target-specific delivery in the current field of nanomedicine.

Figure 12A and 12B reveals the mice tumor section before and after the PMS nanocomposite treatment. The black arrows indicate that the tumor regions in nontreated (Figure 12A) and in the tumor regions disappear in the mice that were treated with PMS nanocomposites (Figure 12B). Figure 12C and 12D shows the heart tissue of the mice treated at the final concentration (2 μg/mL) of the TPT, (TPT+MT), and PMS nanocomposites. The free TPT and severe damage occurred when compared to the other treated groups.[54] It was observed that the combined drugs (TPT+MT) reduce side effects during cancer therapy, and PMS nanocomposites did not cause any side effects in mice cardiocytes. Also, the PMS nanomaterials are capable of killing tumor cells with high efficiency, whereas in the case of free drug-treated mice, although the highest TPT concentration was found in tumor tissue, a substantial amount

DOI: 10.1021/acsomega.7b00978
ACS Omega 2017, 2, 7959−7975

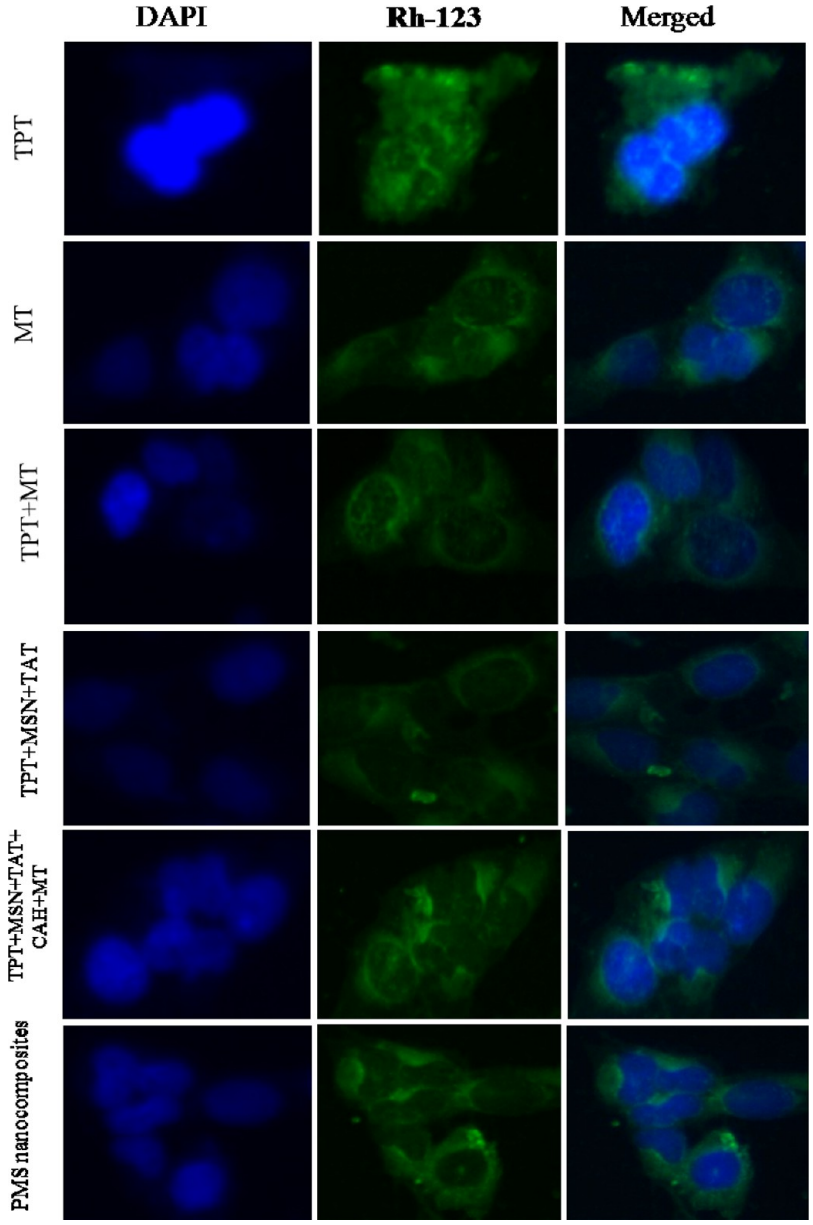

Figure 8. Fluorescence images of PMS nanocomposite treated MDA-MB-231 cells incubated at 37 °C: (right) DAPI stained images, (middle) FITC images, and (left) merged images. Scale bar 50 μm.

was accumulated in the liver and heart, inducing severe cardiotoxicity.

Figure 13 depicted the breast tumor bearing mice treated with TPT, MT, TPT+MT, TPT-MSN-TAT-CAH-MT, and PMS nanocomposites. After 24 days treatment, the mice were sacrificed, and the breast tumor regions were collected. The breast tumor samples revealed the effectiveness of treatment with different nanodrug formulations. Among them, the PMS nanocomposite reduced the tumor cell population at large in lobular regions of breast tumor bearing mice. These results indicate that the dual drug loaded PMS nanocomposite directed uniquely with dual targets produced a significant cancer therapeutics strategy.

CONCLUSION

To sum up the present findings, a successful TAT-conjugated PMS nanocomposite to realize efficient delivery of TPT and MT for targeting cell nuclei and cytoplasm was developed. In view of the literature survey, this is the first attempt in chemotherapeutic drug delivery at a distinct subcellular manner with MSN, but it also displayed significant cellular uptake by MDA-MB-231 cells. The *in vitro* cellular uptake process was visualized by CLSM and bio-TEM images. The capabilities of PMS nanocomposites release MT in the cytoplasm due to disassembled anionic PAA and CAH in response to acidic pH. Subsequently, TAT conjugated on TPT-MSN could facilitate translocation to the nucleus, resulting in facile release of active drug TPT. In addition, released drugs from the PMS nanocomposites had preponderant cytotoxicity on breast cancer cells. We also confirmed the good biocompatibility and tumor suppression of PMS nanocomposites that inhibit tumor growth even with negligible acute toxicity. The designed PMS accomplishes precise delivery of discrete therapeutic efficacy to their individual sites for achieving efficient synergistic cancer therapy with reduced tumor populations in the mice model. Conclusively, the present findings would bring the

DOI: 10.1021/acsomega.7b00978
ACS Omega 2017, 2, 7959−7975

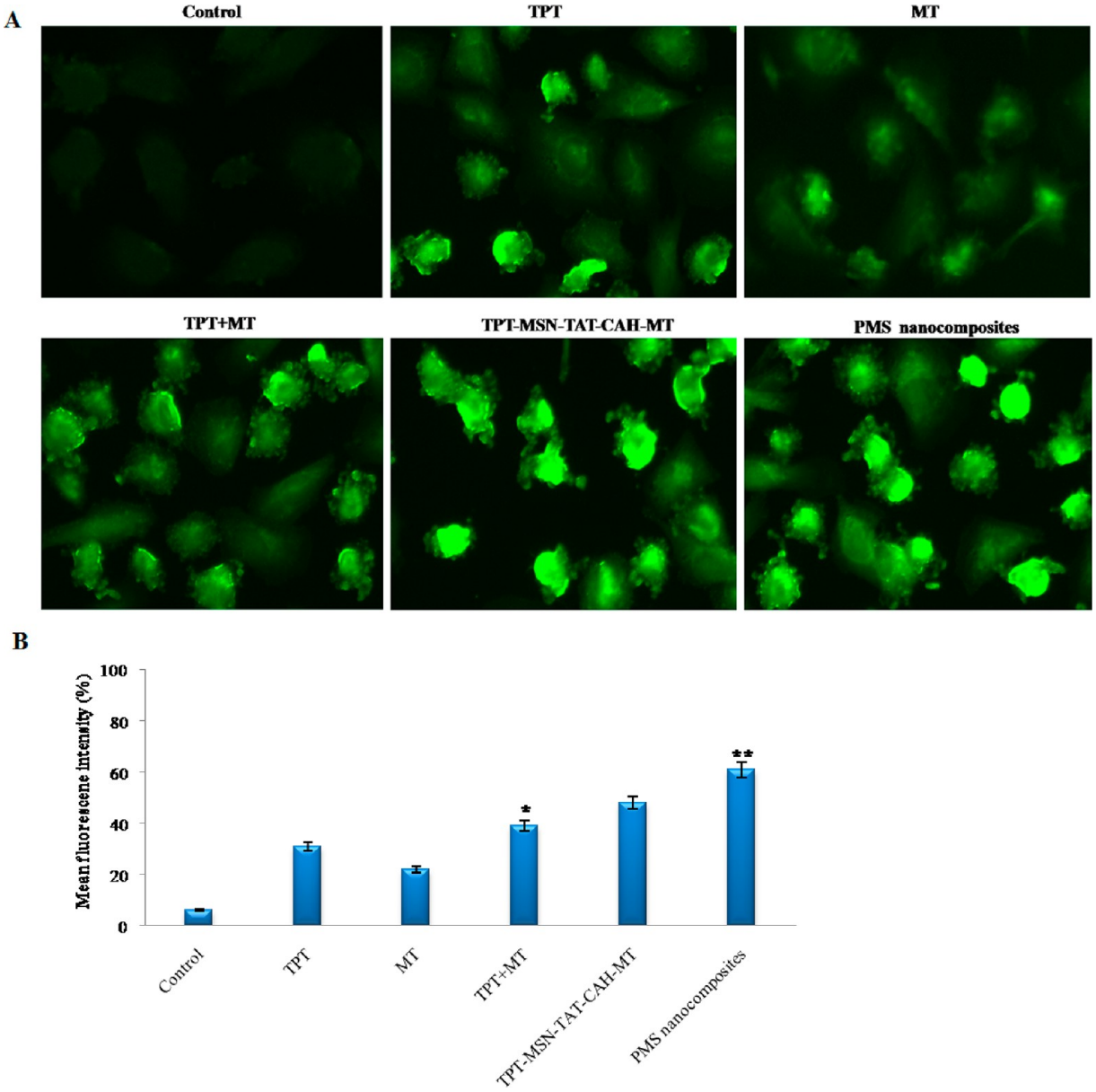

Figure 9. (A) Fluorescence images of MDA-MB-231 cells after treatment by nanodrug formulations and stained with DCFH-DA showed the effects on ROS generation. (B) The quantitative analysis of ROS generation using a plate reader in MDA-MB-231 cells. The data stand for mean ± SD, $*p \leq 0.05$ was calculated statistically significant. Scale bar 400× magnifications.

functionalized PMS nanocomposite, a prominent versatile drug carrier which could act as an alternative in drug delivery for efficient targeting of breast cancer. Thus, it holds a key that unlocks the promise of breast cancer medicine.

EXPERIMENTAL SECTION

Chemicals. Hexadecyl trimethylammonium chloride (CTAC), sodium hydroxide (NaOH), tetraethyl orthosilicate (TEOS), (3-aminopropyl) triethoxysilane (APTES), poly-(acrylic acid) (PAA), *N*-hydroxysuccinimide (NHS), citraconic anhydride (CAH), (4,6-diamidino-2-phenylindole) (DAPI), paraformaldehyde, *N*-(3-(dimethylamino)-propyl)-3-ethyl carbodiimide (EDC), 2′,7′-dichlorofluorescein diacetate (DCFH-DA), rhodamine-123, fluorescein isothiocyanate (FITC) conjugated TAT (FITC-TAT), metformin (MT), and topotecan (TPT) were purchased from Sigma-Aldrich (India).

Synthesis of MSN Nanoparticles. The general route for the synthesis of MSN-NH_2 was carried out by the previously described protocol.[55] Typically, CTAC (0.25 g) and NaOH (50 μL, 2 M) were added into 150 mL of distilled water and gradually stirred at 80 °C for 1 h. Then, TEOS (1 mL) was introduced successively into the reaction solution, by continuously stirring at 80 °C for 3 h. The synthesized nanoparticles were centrifuged and purified by deionized water and methanol and dried overnight. Consequently, the product was refluxed to remove the surfactant (CTAC) by adding 1.5 mL of HCl, 20 mL of methanol, and 1% sodium chloride (NaCl) at 80 °C for 5 h. Final products were obtained by centrifugation and washed thoroughly with ethanol and dried overnight.

The MSN nanoparticles were heated at 80 °C for 3 h, and APTES (5 mL) was added to modify the surface of MSNs with

DOI: 10.1021/acsomega.7b00978
ACS Omega 2017, 2, 7959−7975

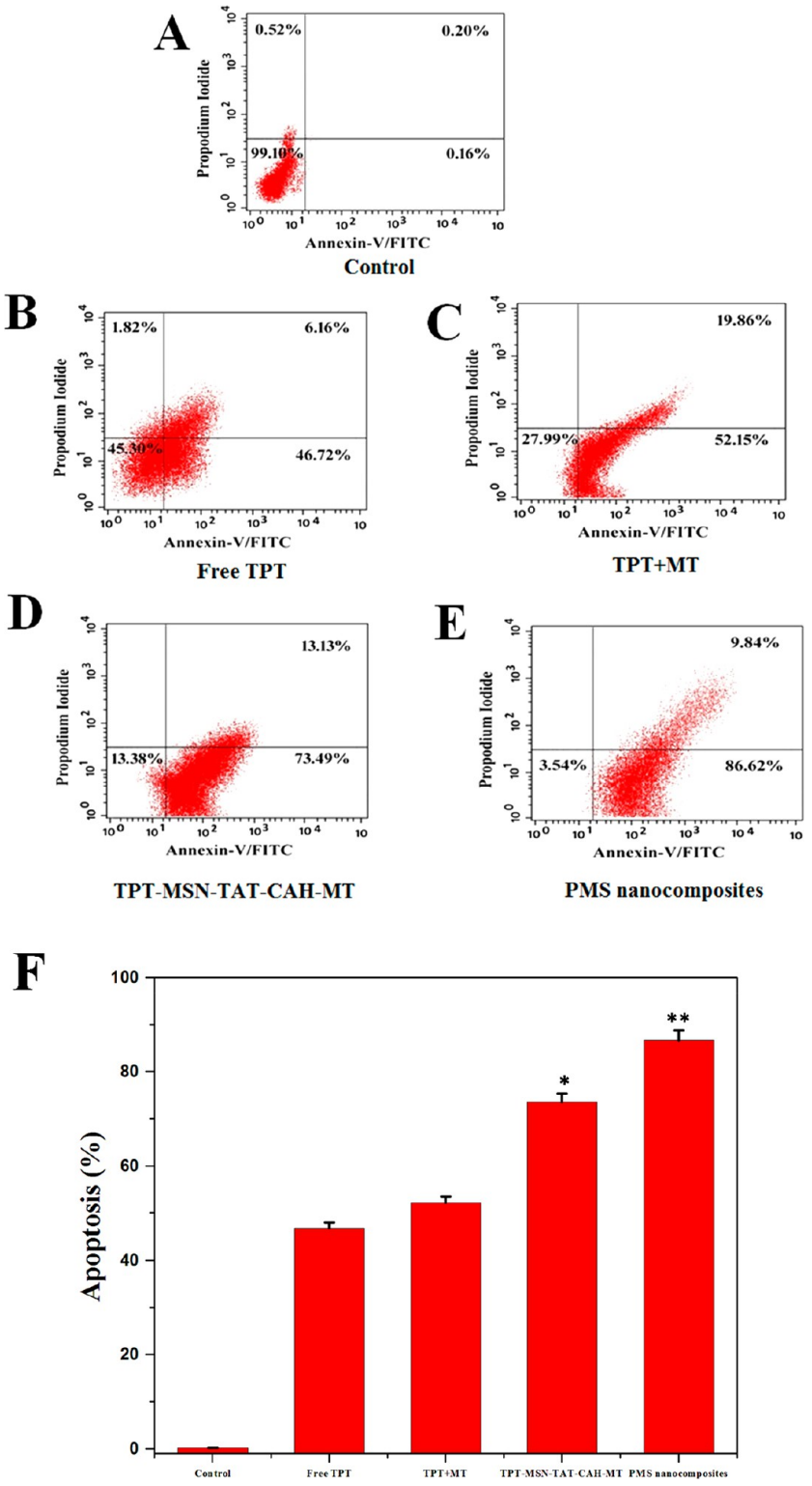

Figure 10. (A–E) Flow cytometry of apoptotic MDA-MB-231 breast cancer cells as assessed by Annexin V-FITC/PI staining. (F) The percentage of apoptotic cells in treatment of cancer cells by different drug components. The data represent mean ± SD, and $*p \leq 0.05$ value is assumed to be statistically significant.

amine groups. The final products were centrifuged and rinsed with ethanol and deionized water.

Topotecan-Loaded MSN-NH_2. An amount of 100 mg of MSN-NH_2 and topotecan hydrochloride (1 mg/mL) was successively introduced into 10 mL of PBS (10 mM, pH 7.4). Afterwards, the solution was reacted at room temperature under stirring overnight. The final product was isolated by gradient centrifugation and rinsed with PBS three times. The TPT-loaded MSN-NH_2 was stored in a refrigerator at 4–8 °C until further use. The loading efficacy of drug in nanoparticles was measured by a UV–vis spectrometer at 510 nm, similar to a method reported previously.[3]

DOI: 10.1021/acsomega.7b00978
ACS Omega 2017, 2, 7959–7975

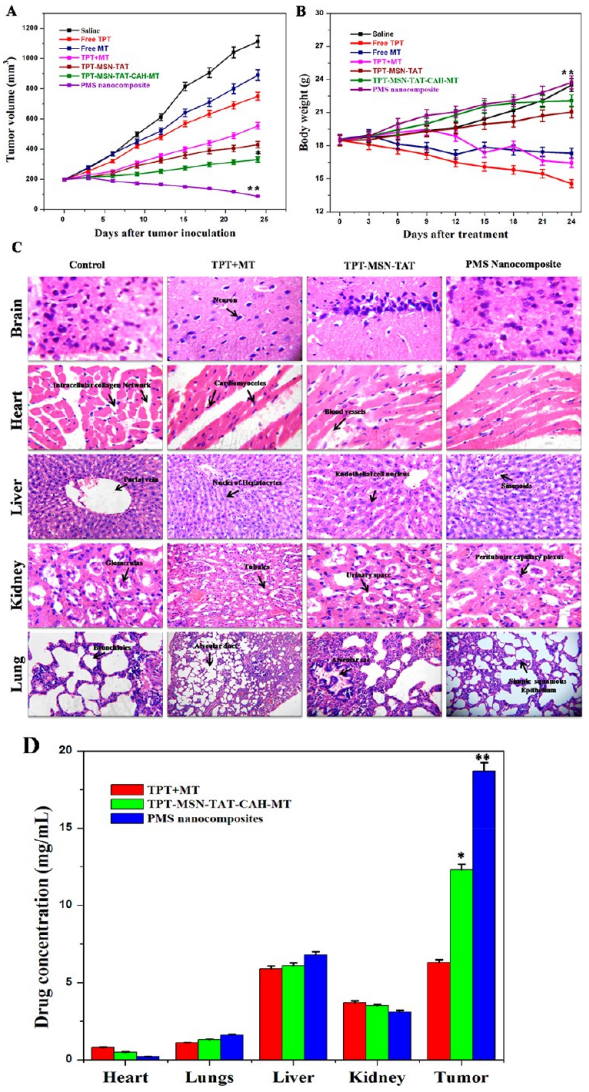

Figure 11. *In vivo* study reveals the noncytotoxicity of formulated nanomaterials in vital organs and their efficacy in minimizing tumor growth. (A) Tumor volume. (B) Body weight of mice treated with saline, TPT, MT, TPT+ MT, TPT-MSN-TAT, TPT-MSN-TAT-CAH-MT, and PMS nanocomposites after 24 days. (C) Hematoxylin and eosin staining of breast cancer induced mice tissue section collected from different groups of mice after 24 days of treatment and (D) the PMS uptake by different intracellular organs of dissected mice. $p \leq 0.05$ value assumes statistically significant.

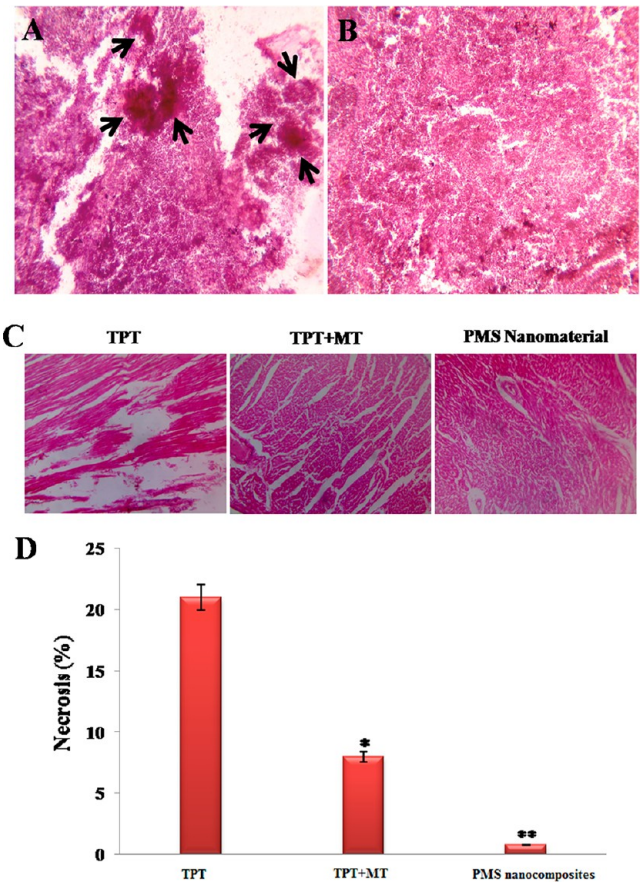

Figure 12. H&E staining of breast tissue section of mice (A) before and (B) after treatment. (C) Mice heart tissue sections, treated with TPT, TPT+MT, and PMS nanocomposites at a final concentration (2 μg/mL), and the free drug induces severe cardiotoxicity effects, when compared to other treatment groups. (D) The necrosis percentage of heart cells in tumor bearing mice subjected to various treatments. Error bars are based on SE of the mean for $n = 3$.

TAT Conjugation with TPT-MSN-NH_2. To form TPT-MSN-TAT, 50 mg of MSNs was dissolved in 10 mL of PBS (pH 7.4), into which 0.5 mg of FITC-TAT was slowly added. Then, 0.3 mM EDC and 0.6 mM NHS were added and stirred at 37 °C for 6 h to activate the carboxylic group of TAT. Unreacted TAT-FITC, EDC, and NHS were separated by centrifugation. The excess TAT-FITC was calculated by UV−vis spectra at the peak of 495 nm.

Synthesis of PAA-cRGD Peptide Combination. To form PAA-cRGD, typically, 4 mgof EDC and 6 mg of NHS were added into 10 mL of PBS; further, 20 mg of PAA was introduced, by stirring for 6 h. Then, 5.5 mg of cRGD was added to the reaction mixture and stirred continuously for 6 h. Then, the final product was harvested by centrifugation and repeatedly purified by deionized water and ethanol.

Preparation of CAH-MT combination. To synthesize CAH-MT, 40 mg CAH and 60 mg MT were added to 5 mL of HEPES buffer (pH 7.2). The reaction products was stirred for 12 h and harvested by centrifugation and purified by distilled water.

Preparation of PMS Nanocomposite. Typically, 50 mg of TPT-MSN-TAT was gradually added in PBS (pH 7.4); subsequently EDC (0.2 mM) and NHS (0.5 mM) were added and allowed overnight. Then, 10 mg of PAA-cRGD and 30 mg of CAH-MT were introduced to the reaction mixture and stirred for 12 h. Finally, the prepared PMS nanocomposites were freeze-dried.

Characterization of Different Mesoporous Silica Nanocomposites. The size and morphological structure of samples were examined under TEM (JEOL JEM 2100 TEM electron microscope). The size distribution and surface charge of functionalized mesoporous silica nanocomposites in a suspension were measured on a Zeta-sizer nanoparticle analyzer (Malvern). The stability of PMS nanocomposites in 10% mouse serum in DMEM (v/v) or 0.01 M PBS (pH 7.4) at 37 °C for 48 h was tested by dynamic light scattering (DLS). The surface analysis was employed by N_2 adsorption isotherms at 77 K (Micromeritics ASAP2020 absorptiometer). The particle surface areas were assessed by the BET (Brunauer−Emmett−Teller) method and Barrett−Joyner−Halenda (BJH) method

DOI: 10.1021/acsomega.7b00978
ACS Omega 2017, 2, 7959−7975

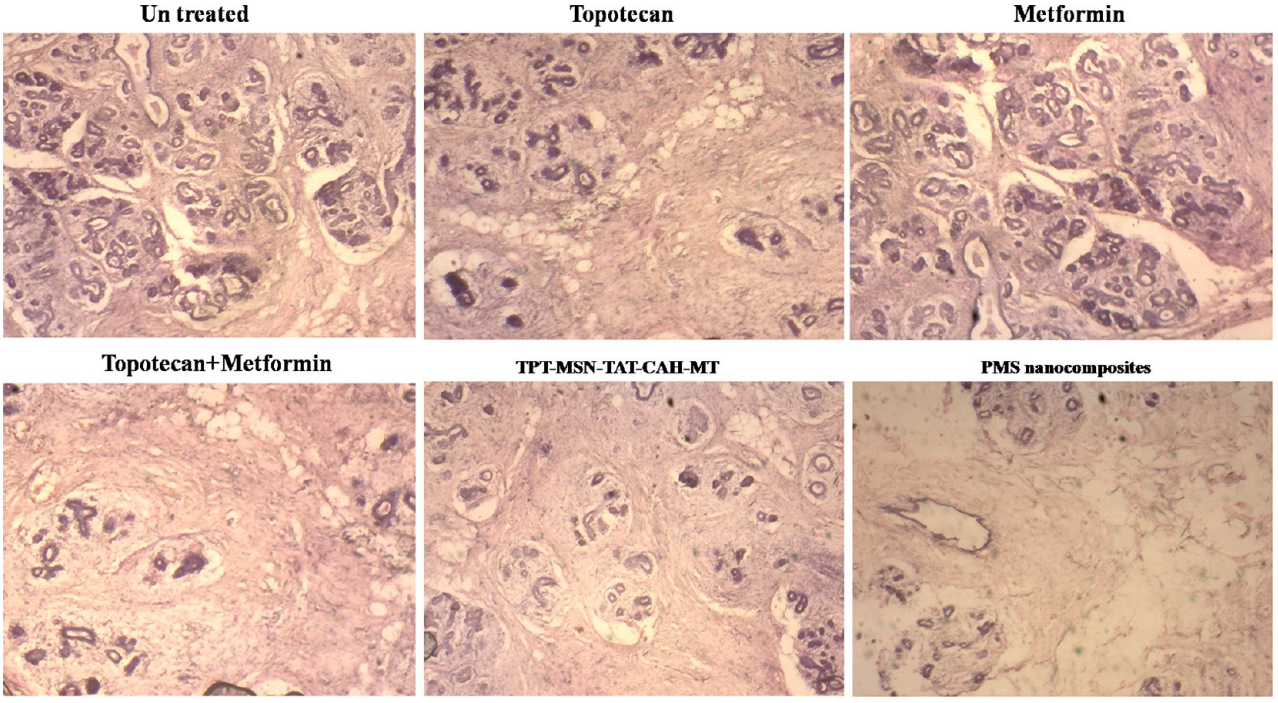

Figure 13. H&E staining of different nanodrug formulation treated lobular regions of breast tumor bearing mice sections obtained from various groups of mice after 24 days treatment.

used to calculate the pore size distributions of particles. FTIR spectroscopy was used to investigate the functional groups at range of 500−4000 cm^{-1} in functionalized MSNs (Thermo Scientific NICOLET 5700).

***In Vitro* Release of TPT and MT from PMS Nanocomposite.** In the drug release experiment, 100 mg of PMS nanocomposite was suspended in a phosphate buffer saline (PBS) solution (1 mL) at corresponding solution with varied pH (pH 7.4, 7.3, 6.8, 5.5, and 4.8), which was enclosed by a dialysis bag (Mw = 14 000). Furthermore, the dialysis setup was immersed in 10 mL of PBS at 37 °C for 3 h under magnetic stirring, and 1 mL of PBS was taken out from the beaker at different time intervals, followed by replacing the equal amount of fresh solution (PBS). Finally, the volume of drug discharged from PBS solution was measured using a UV−vis spectrophotometer at the wavelength of 200−230 nm for MT and 480−510 nm for TPT. The drug loading efficacy of PMS nanocomposite was calculated as previously reported.[56,57]

***In Vitro* Cytotoxic Assay.** Cytotoxicity study was carried out by an MTT assay. In brief, HBL-100 and MDA-MB-231 and MCF-7 cells were pipeted to a 96-well plate (5×10^3 cells/each well) in 90% DMEM medium for a fixed time at 37 °C (5% CO_2). After incubation for 24 h, the different concentrations (0.05, 0.1, 0.2, 0.4, 0.8, 1.0, and 2.0 μg/mL) of TPT, MT, TPT+MT, TPT-MSN-TAT, TPT-MSN-TAT-CAH-MT, and PMS nanocomposite were added. Then, 5 mg/mL of 3-(4, 5-dimethylthiazol-2-yl)-2,5-diphenyltetrazolium bromide (MTT, 100 μL) solution was supplied and allowed to incubate for 4 h. Finally, the produced formazan was diluted in 100 μL of DMSO and observed at 570 nm using an ELISA analyzer (SPR-960).

Analysis of Cellular Uptake of PMS Nanocomposites by CLSM. The internalization of PMS nanocomposites into MDA-MB-231 cells was evaluated by confocal laser scanning microscopy (CLSM). Culture cells were pipetted to 6-well plates (5×10^3 cells/well) and permitted to adhere for 24 h. Then, the cell line was rinsed with PBS and incubated with PMS nanocomposites (IC_{50} concentration) for different intervals (6, 12, 18, and 24 h) and fixed with 4% paraformaldehyde for 1 h. The treated cells were observed on a CLSM (Carl Zeiss LSM 700).

Bio-TEM Observation. The endocytosis of PMS nanocomposites was observed under bio-TEM. The cells were pipetted to 6-well plates (5×10^3 cells/well) and allowed to complete adhesion. After, the cells were incubated with PMS nanocomposites for 24 h, after rinsing in PBS and fixed 2.5% glutaraldehyde at 4 °C overnight. Then, unbound PMS nanocomposite was removed by using PBS solution and fixed in epoxy resin and processed for thin-sectioning using an ultramicrotome (thickness of 50−70 nm). Finally, sliced sections were stained with 2% lead citrate and 5% uranyl acetate for 30 min and observed by JEM-2100.

Analysis of Rhodamine 123 and DAPI Staining. The MDA-MB-231 cells were cultured in a 6-well plate (2×10^3 cells/well), and independent treatment was performed with TPT, MT, TPT+MT, TPT-MSN-TAT-CAH-MT, and PMS nanocomposites for 24 h and fixed with a diluted concentration of nuclear staining DAPI (0.2 μg/mL) for 20 min at 37 °C. Besides, these experimental cells were also treated independently with 0.2 μg/mL of tracker dye Rh-123 and rinsed with PBS solution and observed under a fluorescence microscope (Nikon Eclipse 80i).

Evaluate the ROS Accumulation. The intracellular concentration of mean fluorescent intensity of DCF at emission and excitation wavelengths for quantitative assumption of peroxide and superoxide free radicals was evaluated by pipetting 2 μg/mL of DCFH-DA (2′,7′-dichlorofluorescein diacetate) to a 6-well plate (2×10^3 cells/well), and independent treatment was performed with 2 μg/mL of TPT, MT, TPT+MT, TPT-MSN-TAT-CAH-MT, and PMS nanocomposites for 24 h at 37 °C, respectively. Intracellular ROS accumulation was assessed by a fluorescence microscope (Nikon Eclipse).

DOI: 10.1021/acsomega.7b00978
ACS Omega 2017, 2, 7959−7975

Flow Cytometric Analysis. The effective treatment of TPT, TPT+MT, TPT-MSN-TAT-CAH-MT, and PMS nanoparticles (IC_{50} concentrations) on the induction of apoptosis in the cancer cell line was assessed by a flow cytometer using marker vital dyes (annexin V/FITC and propidium iodide (PI)). Then, the treated cells were mixed with 100 μL of binding buffer and followed by 2 μL of annexin V-FITC and 5 μL of PI. The mixture was then incubated for 20 min in lack of light at room temperature and observed under a flow cytometer (BD, FACS Calibur, USA).

Assessment of Antitumor Activity. For evaluating the *in vivo* treatment efficacy of different particles and drugs, athymic nude female mice around 18−21 g were used to investigate tumor volume, body weight, and effects of *in vivo* antitumor activity. First, the nude mice were subcutaneously injected with five million MDA-MB-231 breast cancer cells. After, the tumor average diameter was reached at 200 mm^3; the mice were randomly divided into 5 groups (four mice per group). The different experimental mice groups were intravenously injected with saline, TPT, MT, TPT+MT, TPT-MSN-TAT, TPT-MSN-TAT-CAH-MT, and PMS nanocomposite, respectively, and a dose of 5 mg/kg was administered every 3 days. The mice were observed up to 24 days. The measurement of tumor size and body weight calculation was performed every 3 days using the following formula: $TV = (L - W2)/2$, with W being smaller than L. After the therapeutic experiment, the treated nude mice were sacrificed using a CO_2 inhalation method and the major organ samples (brain, heart, liver, kidney, and lung) and breast cancer tissue sections excised from necropsy and embedded in 10% formalin. Then, each organ was independently embedded in paraffin, and thin-sectioning (4 μm) of organ samples was placed and stained with H&E (hematoxylin and eosin). The images were collected using a light microscope (Olympus, BH-2). All of the above-mentioned animal experiments were executed with complete protocols permitted by the IACUC (Institutional Animal Care and Use Committees) guidelines.

Statistical Analysis. The value of each experiment was independently conducted and performed in triplicate, and the data were assessed using a mean ± standard error and student's t test. The significance was statistically considered if $p^* < 0.05$.

■ ASSOCIATED CONTENT

Supporting Information

The Supporting Information is available free of charge on the ACS Publications website at DOI: 10.1021/acsomega.7b00978.

Stability of PMS nanocomposite and TPT drug molecule discharging profile at nuclear pH (PDF)

■ AUTHOR INFORMATION

Corresponding Author

*E-mail: sknanomedpu@gmail.com; sk_protein@periyaruniversity.ac.in.

ORCID

Soundarapandian Kannan: 0000-0003-0207-1577

Notes

The authors declare no competing financial interest.

■ ACKNOWLEDGMENTS

This work was financially supported by UGC-MRP, (Grant number F. No-43-581/2014(SR)) Govt. of India. We thank the EM facility center (All India Institute of Medical Sciences), New Delhi, for EM analysis.

■ REFERENCES

(1) Decuzzi, P.; Godin, B.; Tanaka, T.; Lee, S. Y.; Chiappini, C.; Liu, X.; Ferrari, M. Size and Shape Effects in the Biodistribution of Intravascularly Injected Particles. *J. Controlled Release* **2010**, *141*, 320−327.

(2) Li, M.; Deng, H.; Peng, H.; Wang, Q. Functional nanoparticles in targeting glioma diagnosis and therapies. *J. Nanosci. Nanotechnol.* **2014**, *14*, 415−32.

(3) Murugan, C.; Rayappan, K.; Thangam, R.; Bhanumathi, R.; Shanthi, K.; Vivek, R.; Thirumurugan, R.; Bhattacharyya, A.; Sivasubramanian, S.; Gunasekaran, P.; Kannan, S. Combinatorial nanocarrier based drug delivery approach for amalgamation of anti-tumor agents in breast cancer cells: an improved nanomedicine strategy. *Sci. Rep.* **2016**, *6*, 34053.

(4) Kang, X.; Wang, H.; Peng, H.; Chen, B.; Zhang, W.; Wu, A.; Xu, Q.; huang, Y. Codelivery of dihydroartemisinin and doxorubicin in mannosylated liposomes for drug-resistant colon cancer therapy. *Acta Pharmacol. Sin.* **2017**, *38*, 885−896.

(5) Zhang, J.; Wang, L.; Chan, H. F.; Xie, W.; Chen, S.; He, C.; Wang, Y.; Chen, M. Co-delivery of paclitaxel and tetrandrine via iRGD peptide conjugated lipid-polymer hybrid nanoparticles overcome multidrug resistance in cancer cells. *Sci. Rep.* **2017**, *7*, 46057.

(6) Chang, R. S.; Suh, M. S.; Kim, S.; Shim, G.; Lee, S.; Han, S. S.; Lee, K. E.; Jeon, H.; Choi, H. G.; Choi, Y.; Kim, C. W.; Oh, Y. K. Cationic drug derived nanoparticles for multifunctional delivery of anticancer siRNA. *Biomaterials* **2011**, *32*, 9785−9795.

(7) Zheng, C. F.; Zheng, M. B.; Gong, P.; Deng, J. Z.; Yi, H. Q.; Zhang, P. F.; Liu, P.; Ma, Y.; Cai, L. Polypeptide cationic micelles mediated co-delivery of docetaxel and siRNA for synergistic tumor therapy. *Biomaterials* **2013**, *34*, 3431−3438.

(8) Han, L.; Tang, C.; Yin, C. Dual-targeting and pH/redox-responsive multi-layered nanocomplexes for smart co-delivery of doxorubicin and siRNA. *Biomaterials* **2015**, *60*, 42−52.

(9) Lee, J. E.; Lee, N.; Kim, T.; Kim, J.; Hyeon, T. Multifunctional mesoporous silica nanocomposite nanoparticles for theranostic applications. *Acc. Chem. Res.* **2011**, *44*, 893−902.

(10) Xue, M.; Zhong, X.; Shaposhnik, Z.; Qu, Y.; Tamanoi, F.; Duan, X.; Zink, J. I. pH-Operated Mechanized Porous Silicon Nanoparticles. *J. Am. Chem. Soc.* **2011**, *133*, 8798−8801.

(11) Alberti, S.; Soler-Illia, G.; Azzaroni, O. Gated supramolecular chemistry in hybrid mesoporous silica nanoarchitectures: controlled delivery and molecular transport in response to chemical, physical and biological stimuli. *Chem. Commun.* **2015**, *51*, 6050−6075.

(12) Chen, L.; Zhou, X.; Nie, W.; Zhang, Q.; Wang, W.; Zhang, Y.; He, C. Multifunctional Redox-Responsive Mesoporous Silica Nanoparticles for Efficient Targeting Drug Delivery and Magnetic Resonance Imaging. *ACS Appl. Mater. Interfaces* **2016**, *8*, 33829−33841.

(13) Arap, W.; Pasqualini, R.; Ruoslahti, E. Cancer treatment by targeted drug delivery to tumor vasculature in a mouse model. *Science* **1998**, *279*, 377−380.

(14) Kang, B.; Megan, A. M.; Mostafa, A. E. Nuclear Targeting of Gold Nanoparticles in Cancer Cells Induces DNA Damage, Causing Cytokinesis Arrest and Apoptosis. *J. Am. Chem. Soc.* **2010**, *132*, 1517.

(15) Nakielny, S.; Dreyfuss, G. Transport of proteins and RNAs in and out of the nucleus. *Cell* **1999**, *99*, 677.

(16) Patel, S. S.; Belmont, B. J.; Sante, J. M.; Rexach, M. F. Natively unfolded nucleoporins gate protein diffusion across the nuclear pore complex. *Cell* **2007**, *129*, 83.

(17) Alber, F.; Dokudovskaya, S.; Veenhoff, L. M.; Zhang, W.; Kipper, J.; Devos, D.; Suprapto, A.; Karni-Schmidt, O.; Williams, R.; Chait, B. T.; et al. The molecular architecture of the nuclear pore complex. *Nature* **2007**, *450*, 695.

(18) Kubitscheck, U.; Grnwald, D.; Hoekstra, A.; Rohleder, D.; Kues, T.; Siebrasse, J. P.; Peters, R. J. Nuclear transport of single molecules: dwell times at the nuclear pore complex. *J. Cell Biol.* **2005**, *168*, 233.

DOI: 10.1021/acsomega.7b00978
ACS Omega 2017, 2, 7959−7975

(19) Pan, L.; He, Q.; Liu, J.; Chen, Y.; Ma, M.; Zhang, L.; Shi, J. Nuclear-Targeted Drug Delivery of TAT Peptide-Conjugated Monodisperse Mesoporous Silica Nanoparticles. *J. Am. Chem. Soc.* **2012**, *134*, 5722−5725.
(20) Gu, Y. J.; Cheng, J.; Lin, C. C.; Lam, Y. W.; Cheng, S. H.; Wong, W. T. Nuclear penetration of surface functionalized gold nanoparticles. *Toxicol. Appl. Pharmacol.* **2009**, *237*, 196−204.
(21) Gratton, S. E. A.; Ropp, P. A.; Pohlhaus, P. D.; Luft, J. C.; Madden, V. J.; et al. The effect of particle design on cellular internalization pathways. *Proc. Natl. Acad. Sci. U. S. A.* **2008**, *105*, 11613−11618.
(22) de Jong, W.; Borm, P. J. A. Drug delivery and nanoparticles: Applications and hazards. *Int. J. Nanomed.* **2008**, *3*, 133−149.
(23) Andre, E.; Madler, L.; Velegol, D.; Xia, T.; Eric, M.; Hoek, V.; Somasundaran, P.; Klaessig, F.; Castranova, V.; Thompson, M. Understanding biophysicochemical interactions at the nano−bio interface. *Nat. Mater.* **2009**, *8*, 543−557.
(24) Li, L.; Guan, Y.; Liu, H.; Hao, N.; Liu, T.; Meng, X.; Fu, C.; Li, Y.; Qu, Q.; Zhang, Y.; Ji, S.; Chen, L.; Chen, D.; Tang, F. Silica Nanorattle-Doxorubicin-Anchored Mesenchymal Stem Cells for Tumor-Tropic Therapy. *ACS Nano* **2011**, *5*, 7462−7470.
(25) Cetin, M.; Atila, A.; Sahin, S. and Imran. Preparation and characterization of metformin hydrochloride loaded-Eudragit®RSPO and Eudragit®RSPO/PLGA nanoparticles. *Pharm. Dev. Technol.* **2013**, *18*, 570−576.
(26) Xing, L.; Zheng, H.; Cao, Y.; Che, S. Coordination polymer coated mesoporous silica nanoparticles for pH-responsive drug release. *Adv. Mater.* **2012**, *24*, 6433−6437.
(27) Wu, K.; Cheng, R.; Zhang, J.; Meng, F.; Deng, C.; Zhong, Z. Micellar Nanoformulation of Lipophilized Bortezomib: High Drug Loading, Improved Tolerability and Targeted Treatment of Triple Negative Breast Cancer. *J. Mater. Chem. B* **2017**, *5*, 5658−5667.
(28) Vivek, R.; Thangam, R.; Nipun Babu, V.; Ponraj, T.; Kannan, S. Oxaliplatin-chitosan nanoparticles induced intrinsic apoptotic signaling pathway: A "smart" drug delivery system to breast cancer cell therapy. *Int. J. Biol. Macromol.* **2014**, *65*, 289−297.
(29) Orij, R.; Postmus, J.; Beek, A. T.; Brul, S.; Smits, G. J. In vivo measurement of cytosolic and mitochondrial pH using a pH-sensitive GFP derivative in Saccharomyces cerevisiae reveals a relation between intracellular pH and growth. *Microbiology* **2009**, *155*, 268−278.
(30) Chen, Y.; Chen, H. R.; Zhang, S. J.; Chen, F.; Zhang, L. X.; Zhang, J. M.; Zhu, M.; Wu, H. X.; Guo, L. M.; Feng, J. W.; et al. Multifunctional Mesoporous Nanoellipsoids for Biological Bimodal Imaging and Magnetically Targeted Delivery of Anticancer Drugs. *Adv. Funct. Mater.* **2011**, *21*, 270−278.
(31) Meng, H.; Liong, M.; Xia, T.; Li, Z. X.; Ji, Z. X.; Zink, J. I.; Nel, A. E. Mesoporous Silica Nanoparticles To Deliver Doxorubicin and P-Glycoprotein siRNA To Overcome Drug Resistance in a Cancer Cell Line. *ACS Nano* **2010**, *4*, 4539−4550.
(32) Gao, W.; Chan, J.; Farokhzad, O. C. pH-Responsive Nanoparticles for Drug Delivery. *Mol. Pharmaceutics* **2010**, *7*, 1913−1920.
(33) Nam, J.; Won, N.; Jin, H.; Chung, H.; Kim, S. pH-Induced Aggregation of Gold Nanoparticles for Photothermal Cancer Therapy. *J. Am. Chem. Soc.* **2009**, *131*, 13639−13645.
(34) Legate, K. R.; Montanez, E.; Kudlacek, O.; Fassler, R. ILK, PINCH and parvin: the tIPP of integrin signalling. *Nat. Rev. Mol. Cell Biol.* **2006**, *7*, 20−31.
(35) Maruyama, K. Intracellular targeting delivery of liposomal drugs to solid tumors based on EPR effects. *Adv. Drug Delivery Rev.* **2011**, *63*, 161−169.
(36) Oba, M.; Fukushima, S.; Kanayama, N.; Aoyagi, K.; Nishiyama, N.; Koyama, H.; Kataoka, K. Cyclic RGD peptide-conjugated polyplex micelles as a targetable gene delivery system directed to cells possessing $\alpha v\beta 3$ and $\alpha v\beta 5$ integrins. *Bioconjugate Chem.* **2007**, *18*, 1415−1423.
(37) Cheng, H.; Zhu, J. Y.; Xu, X. D.; Qiu, W. X.; Lei, Q.; Han, K.; Cheng, Y. J.; Zhang, X. Z. Activable Cell-Penetrating Peptide Conjugated Prodrug for Tumor. Targeted Drug Delivery. *ACS Appl. Mater. Interfaces* **2015**, *7*, 16061−16069.
(38) Bannunah, A. M.; Vllasaliu, D.; Lord, J.; Stolnik, S. Mechanisms of Nanoparticle Internalization and Transport Across an Intestinal Epithelial Cell Model: Effect of Size and Surface Charge. *Mol. Pharmaceutics* **2014**, *11*, 4363−4373.
(39) Zhao, M. X.; Zhu, B. J.; Yao, W. J.; Chen, D. F. Therapeutic effect of quantum dots for cancer treatment. *RSC Adv.* **2016**, *6*, 113791−113795.
(40) Schmaljohann, D. Thermo- and pH-responsive polymers in drug delivery. *Adv. Drug Delivery Rev.* **2006**, *58*, 1655−1670.
(41) Chithrani, B. D.; Ghazani, A. A.; Chan, W. C. Determining the size and shape dependence of gold nanoparticle uptake into mammalian cells. *Nano Lett.* **2006**, *6*, 662−668.
(42) Lu, F.; Wu, S. H.; Hung, Y.; Mou, C. Y. Size effect on cell uptake in well-suspended, uniform mesoporous silica nanoparticles. *Small* **2009**, *5*, 1408−1413.
(43) Shanthi, K.; Vimala, K.; Gopi, D.; Kannan, S. Fabrication of a pH responsive DOX conjugated PEGylated palladium nanoparticle mediated drug delivery system: an in vitro and in vivo evaluation. *RSC Adv.* **2015**, *5*, 44998−45014.
(44) Ahmad, J.; Ahamed, M.; Akhtar, M. J.; Alrokayan, S. A.; Siddiqui, M. A.; Musarrat, J.; Al-Khedhairy, A. A. Apoptosis induction by silica nanoparticles mediated through reactive oxygen species in human liver cell line HepG2. *Toxicol. Appl. Pharmacol.* **2012**, *259*, 160−168.
(45) Zhang, Y.; Ali, S. F.; Dervishi, E.; Xu, Z.; Li, Y.; Casciano, D.; Biris, A. S. Cytotoxicity effects of graphene and single-wall carbon nanotubes in neural phaeochromocytoma-derived PC12 cells. *ACS Nano* **2010**, *4*, 3181.
(46) Smith, P. E. S.; Brender, J. R.; Ramamoorthy, A. Induction of Negative Curvature as a Mechanism of Cell Toxicity by Amyloidogenic Peptides: The Case of Islet Amyloid Polypeptide. *J. Am. Chem. Soc.* **2009**, *131*, 4470−4478.
(47) Vivek, R.; Thangam, R.; Nipun Babu, V.; Rejeeth, C.; Sivasubramanian, S.; Gunasekaran, P.; Muthuchelian, K.; Kannan, S. Multifunctional HER2-Antibody Conjugated Polymeric Nanocarrier-Based Drug Delivery System for Multi-Drug-Resistant Breast Cancer Therapy. *ACS Appl. Mater. Interfaces* **2014**, *6*, 6469−6480.
(48) Chaudhari, R.; Kumar, A. K.; Khandelwal, V. K. M; Ukawala, M.; Manjappa, A. S.; Mishra, A. K.; Monkkonen, J.; Murthy, R. S. R. Bone Metastasis Targeting: A Novel Approach to Reach Bone Using Zoledronate Anchored PLGA Nanoparticle as Carrier System Loaded with Docetaxel. *J. Controlled Release* **2012**, *158*, 470−478.
(49) Chatterjee, K.; Zhang, J.; Honbo, N.; Karliner, J. S. Doxorubicin Cardiomyopathy. *Cardiology* **2010**, *115*, 155−162.
(50) Takemura, G.; Fujiwara, H. Doxorubicin-induced cardiomyopathy from the cardiotoxic mechanisms to management. *Prog. Cardiovasc. Dis.* **2007**, *49*, 330−352.
(51) Xue, C.; Wang, C.; Sun, Y.; Meng, Q.; Liu, Z.; Huo, X.; Sun, P.; Sun, H.; Ma, X.; Ma, X.; Peng, J.; Liu, K. Targeting P-glycoprotein function, p53 and energy metabolism: Combination of metformin and 2-deoxyglucose reverses the multidrug resistance of MCF-7/Dox cells to doxorubicin. *Oncotarget.* **2017**, *31*, 8622−8632.
(52) Veronese, F. M.; Pasut, G. PEGylation, successful approach to drug delivery. *Drug Discovery Today* **2005**, *10*, 1451−1458.
(53) Yamashita, K.; Yoshioka, Y.; Higashisaka, K.; Mimura, K.; Morishita, Y.; Nozaki, M.; et al. Silica and titanium dioxide nanoparticles cause pregnancy complications in mice. *Nat. Nanotechnol.* **2011**, *6*, 321−328.
(54) Xie, G.; Sun, J.; Zhong, G. Tissular localization and excretion of intravenously administered silica nanoparticles of different sizes. *J. Nanopart. Res.* **2012**, *14*, 671.
(55) Lai, C. Y.; Trewyn, B. G.; Jeftinija, D. M.; Jeftinija, K.; Xu, S.; Jeftinija, S.; Lin, V. S. A mesoporous silica nanosphere-based carrier system with chemically removable CdS nanoparticle caps for stimuli-responsive controlled release of neurotransmitters and drug molecules. *J. Am. Chem. Soc.* **2003**, *125*, 4451−4459.

DOI: 10.1021/acsomega.7b00978
ACS Omega 2017, 2, 7959−7975

(56) Vimala, K.; Shanthi, K.; Sundarraj, S.; Kannan, S. Synergistic effect of chemo-photothermal for breast cancer therapy using folic acid (FA) modified zinc oxide nanosheet. *J. Colloid Interface Sci.* **2017**, *488*, 92−108.
(57) Vivek, R.; Nipun Babu, V.; Thangam, R.; Subramanian, K. S.; Kannan, S. pH-responsive drug delivery of chitosan nanoparticles as Tamoxifen carriers for effective anti-tumor activity in breast cancer cells. *Colloids Surf., B* **2013**, *111*, 117−123.

DOI: 10.1021/acsomega.7b00978
ACS Omega 2017, 2, 7959−7975